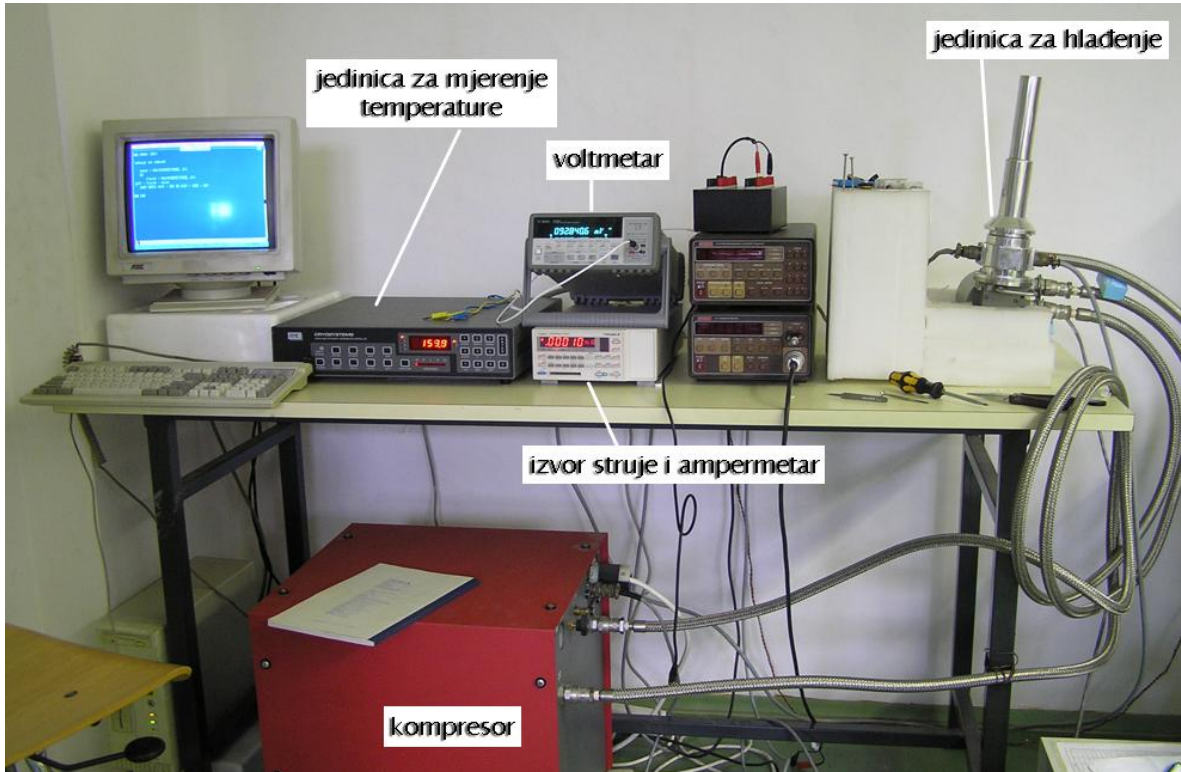
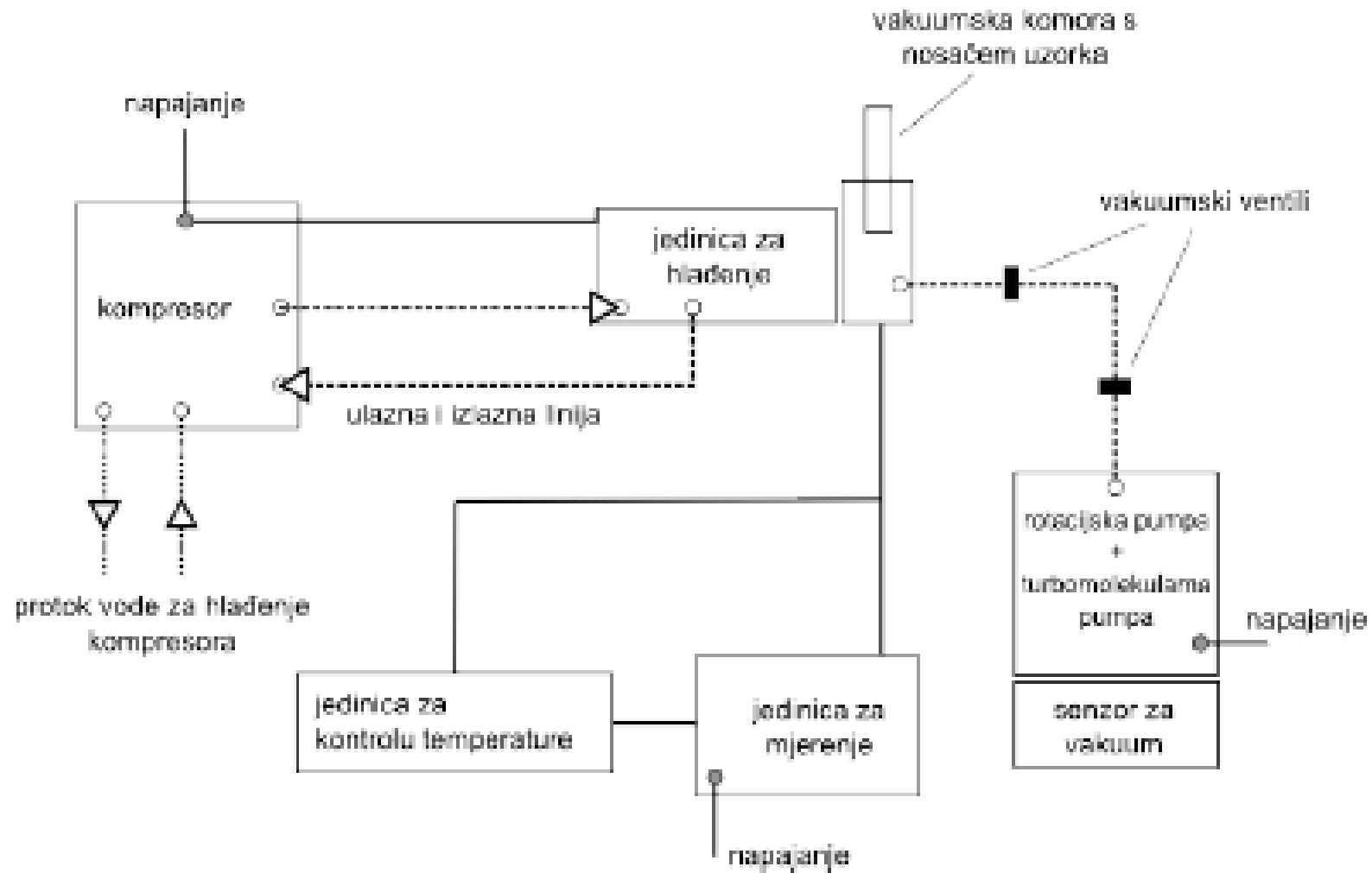


# Postav za mjerjenje otpornosti

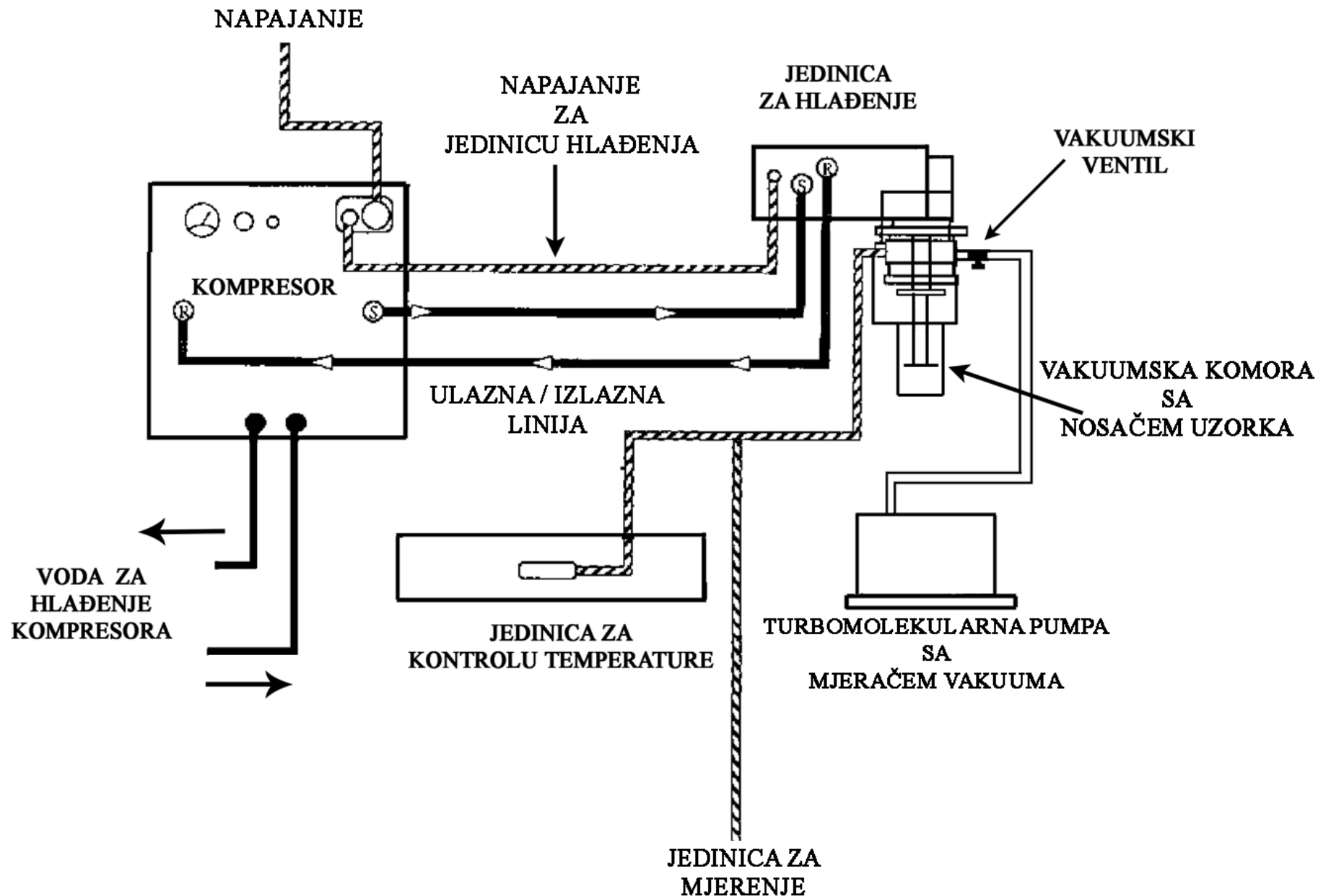


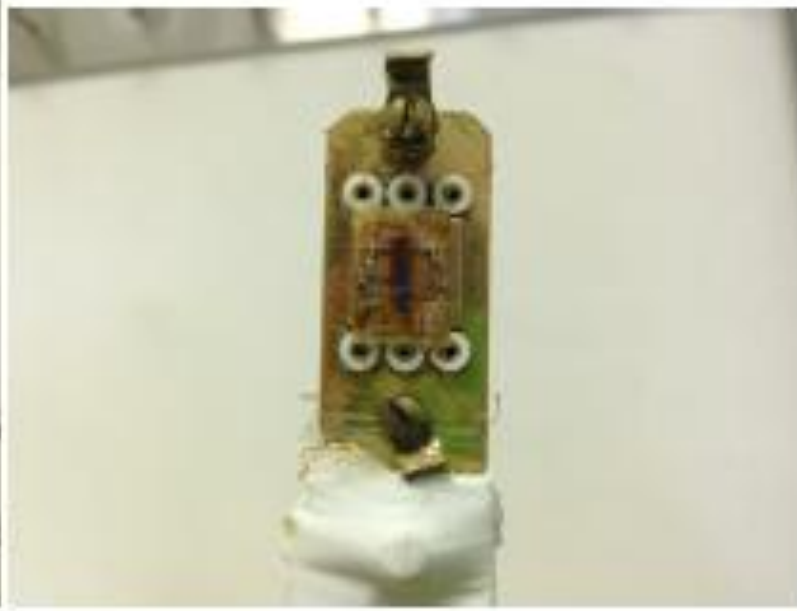
- Merenje istosmjernom strujom, metodom četiri kontakta, u području 10-290 K
- Za hlađenje je korišten hladnjak sa zatvorenim ciklusom (CCR)
- Procesom upravlja prilagođeni računalni program
- Turbomolekularna pumpa održava vakuum ( $10^{-6}$  Pa)
- Silazno i uzlazno temperaturno ovisno mjerjenje napona



Slika 4.15: Shema mjernog postava.

Cijeli postav može se podjeliti na sustav za hlađenje i sustav za mjerjenje.





Slika 4.14: Otvorena komora s uzorkom na stalku.

## Postavljanje kontakata na uzorak

Na uzorak je potrebno postaviti četiri kontakta (dva naponska i dva strujna). Uzorci su izrezani iz trake metalnog stakla dobivene "melt spinning" metodom

Dugi su oko  $5\text{mm}$ , široki  $1.5\text{mm}$  i debeli  $0.03\text{mm}$ , slika (4.14). Kontakti se rade tako da se tanka bakrena žica kontaktno vari na uzorak. Kontaktno varenje radi se s uređajem prikazanim na slici (4.13). U uređaju se nabija kapacitor. Pincetom koja ima bakrene krajeve, koji su spojeni u krug s kapacitorom, pritisne se bakrena žičica na uzorak i zatim se kapacitor, preko sklopke, isprazni i žičica se zavari za uzorak.

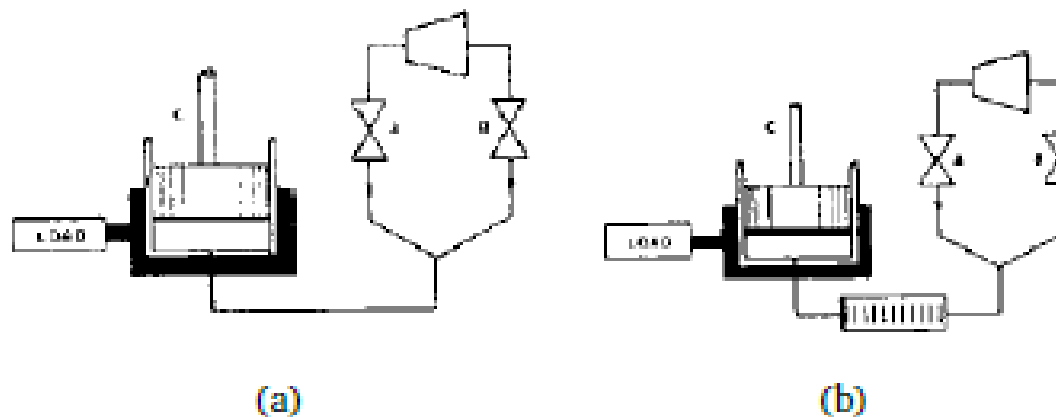


Slika 4.13: Aparat za varenje.

Sustav hlađenja čine helijev hladnjak (CHR), koji se sastoji od kompresora i ras-hladne jedinice te sustava za postizanje vakuma, kojeg čine rotacijska i turbomolekularna vakuumska pumpa i senozr za vakuum.

Helijev hladnjak radi na istom principu kao i obični hladnjak samo što umjesto freona, kao rashladnog plina, koristi helij. Radna temperatura helijevog hladnjaka je, za razliku od običnog, na destak  $K$ . Kompresor se podmazuje uljem i hlađi vodom tijekom rada. Rashladna jedinica se sastoji od cilindra i klipa te dva ventila i radi na manjim brzinama nego kompresor. Kompresor i rashladna jedinica su odvojeni ( $\sim 2m$ ).

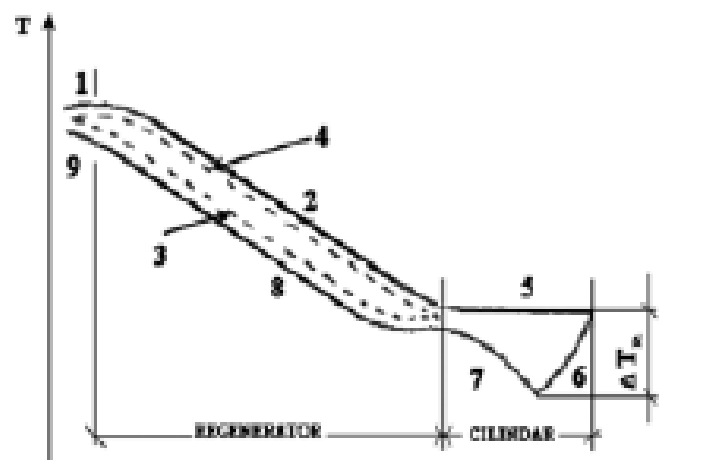
Tok helija u hladnjaku je ciklički, a shema rada prikazana je na slici (4.16).



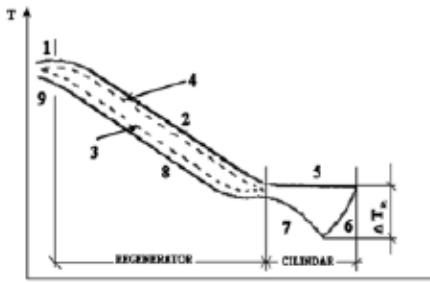
Slika 4.16: Shema rada helijevog hladnjaka. a) bez regeneratora, b) s regeneratorom.

Izvor komprimiranog plina povezan je s cilindrom C preko ulaznog ventila A.

B je izlazni ventil koji propušta plin niskog tlaka natrag u kompresor. U početku ciklusa klip je na dnu cilindra, ventil A se otvara i cilindar se uz podizanje klipa puni komprimiranim plinom. B ventil je zatvoren. Zatim se A ventil zatvara, a B ventil otvara i komprimirani plin ekspandira pri čemu se hlađi. Plin u cilindru je sada hladniji od komore koja se hlađi i ona predaje toplinu plinu preko zidova cilindra. Klip se zatim spušta i ispumpava preostali plin koji odlazi kroz otvoreni B ventil. Međutim, opisani ciklus neće postići željeno hlađenje. Potrebno je ulazni plin ohladiti izlaznim plinom prije nego on uđe u cilindar. To se postiže regeneratorom koji izvlači toplinu iz ulaznog plina, sprema je, i zatim predaju izlaznom plinu. Regenerator je napravljen od materijala velike efektivne površine, velikog toplinskog kapaciteta i male toplinske vodljivosti. Toplinski profil ciklusa s regeneratorom je na slici (4.17).



Slika 4.17: Temperaturni profil ciklusa s regeneratorom.

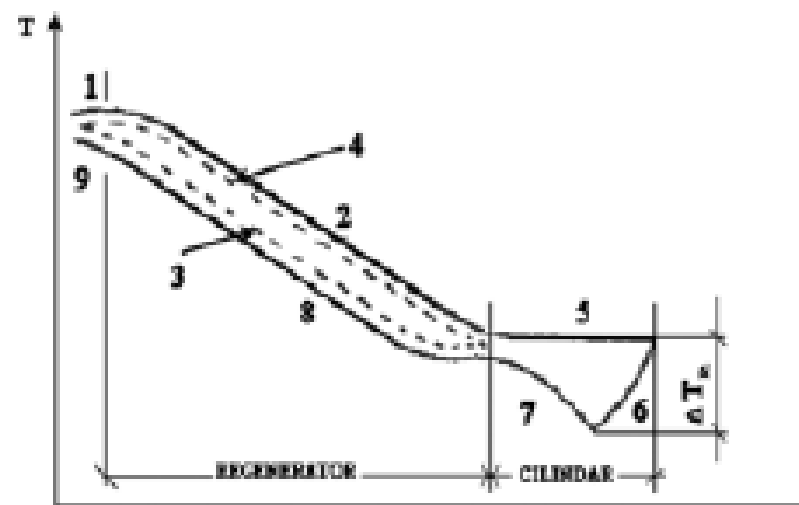


Koraci u ciklusu su sljedeći:

Slika 4.17: Temperaturni profil ciklusa s regeneratorom.

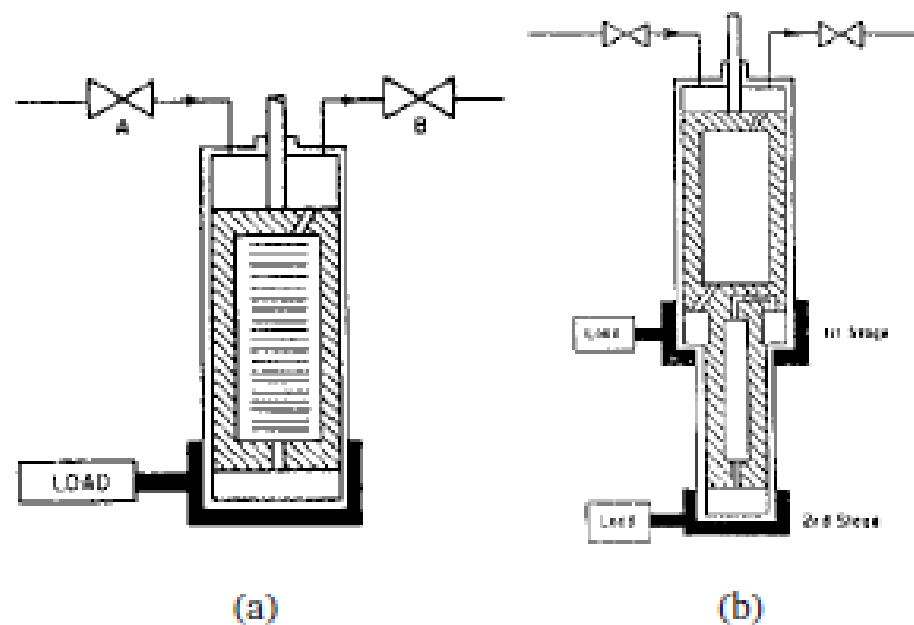
- Klip je na dnu cilindra. Komprimirani plin, sobne temperature, ulazi u kroz ventil A (1).
- Klip se podiže, a plin prolazi kroz regenerator koji apsorbira toplinu iz plina pri čemu se zagrijava (3-4). Plin se hlađi (2).
- Ohlađeni plin pod tlakom puni cilindar. Temperatura plina je sada praktički jednaka temperaturi komore koja se hlađi (5).
- Zatvara se ulazni ventil A, a otvara se izlazni B. Plin ekspandira i dodatno se ohlađi za temperaturu  $\Delta T$  (6).
- Toplina iz komore prolazi preko zidova cilindra na plin i zagrijava ga na temperaturu blisku onoj na kojoj je bio kada je ušao u cilindar (7).
- Prilikom ekspanzije dio plina prolazi kroz regenerator i zagrijava se (8) tako što preuzima toplinu od regeneratora koji se pritom hlađi (4-3).

- g) Klip se spušta i istiskuje ostatak hladnog plina kroz regenerator. Zbog efikasnosti regeneratora koja je manja od 100% uvijek postoji razlika u temperaturi regeneratora i plina pa je izlazni plin, u bilo kojoj točki dijagrama, uvijek malo hladniji nego ulazni plin.
- h) Plin pod niskim tlakom i približno na sobnoj temperaturi napušta jedinicu za hlađenje kroz ventil B (9). Plin odlazi u kompresor gdje se tlači i pri tome održava na sobnoj temperaturi, a zatim ulazi u novi ciklus.



Slika 4.17: Temperaturni profil ciklusa s regeneratorom.

U praksi se regenerator nalazi unutar samog klipa. Cilindar je zatvoren s obje strane, a plin prolazi kroz klip u kojem je regenerator, slika (4.18). Na taj način pojednostavljuje se izvedba rashladne jedinice jer, u ovom slučaju, se tlakovi s dvije strane cilindra brzo izjednače i nije potrebno korištenje visokotlačnih brtvi i sile na klip su puno manje. Sustav s jednim regeneratorom može hladiti na temperature u rasponu od  $30 - 80K$ . Dodavanjem drugog (nekad i trećeg) regeneratora postižu se temperature ispod  $10K$ . U sustavu s dva regeneratora postoje tri prostora unutar cilindra u kojima se plin može nalaziti. Između gornjeg i srednjeg dešava se prvi stupanj hlađenja, a između srednjeg i donjeg drugi stupanj hlađenja, slika (4.18b).



Slika 4.18: Klip s regeneratorom u cilindru. a) jedan regenerator, b) dva regeneratora.

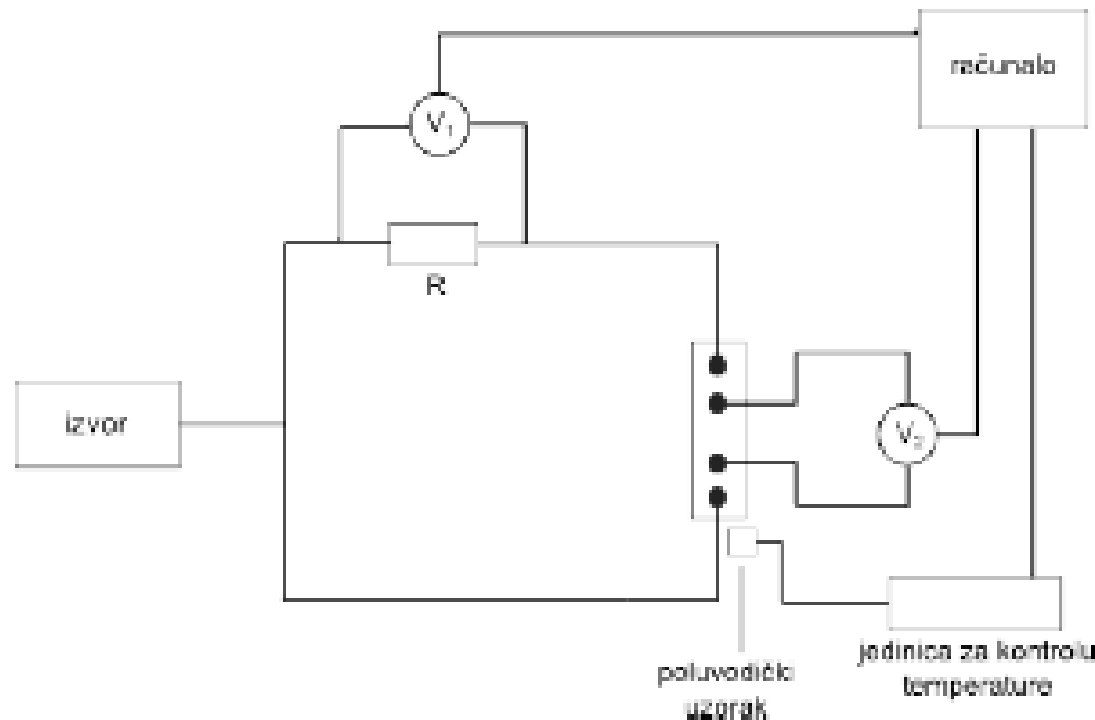
Stalak s uzorkom se nalazi u komori koja se hlađi. Čitavo vrijeme u komori se održava visoki vakuum ( $< 10^{-5} \text{ mbar}$ ). Vakuumom se postiže bolja termalna izolacija, ali se i sprječava utjecaj kondenzata na mjerjenje otpora. Prilikom hlađenja, ukoliko u komori ima vodene pare ili dušika, oni će se kondenzirati na uzorku što će utjecati na mjerjenje. Vakuum se postiže rotacijskom i turbomolekularnom pumpom. Najprije s radom kreće rotacijska pa se na tlaku od oko  $10^{-5} \text{ mbar}$  pali i turbomolekularna pumpa. Stanje vakuuma prati se senzorom za vakuum.



Slika 4.14: Otvorena komora s uzorkom na stalku.

**Sustav za mjerjenje** sastoji se od mjerne jedinice i jedinice za kontrolu temperature. Mjernu jedinicu čine izvor (Yokagava), dva voltmetra (Agilent 34401A), otpornik i računalo. Jedinica za kontrolu temperature (*LakeShore*) mjeri temperaturu uzorka.

Shema sustava za mjerjenje je na slici (4.19).



**Slika 4.19:** Shema postava za mjerjenje otpora.

Gornja shema prikazuje DC metodu mjerena. Na nekoliko uzoraka napravljena je i AC metoda. Kod AC metode korišteno je lock-in pojačalo koje je istovremeno služilo i kao izvor. Općenito AC mjerene pokazivat će manje šuma. Naime, kod DC mjerenja, ukoliko se koriste manje struje (prevelika struja može zagrijati uzorak), mogu se pojaviti određeni kapacitivni doprinosi zbog nehomogene raspodjele struje između kontakata. Kod AC metode takvi doprinosi biti će eliminirani jer lock-in pojačalo može odvojiti samo signal koji je u fazi s referentnim signalom, a taj predstavlja samo Ohmski doprinos otporu koji želimo mjeriti. AC metodom se izbjegava i šum koji dolazi od toga što se, kod DC mjerenja, temperatura između  $+I$  i  $-I$  može razlikovati. Pokazalo se, ipak, da DC metoda sa strujom od  $5mA$  (što i dalje nije prevelika struja) daje gotovo iste rezultate kao i AC metoda za manje struje.

Jedinica za kontrolu temperature ima poluvodički uzorak koji se nalazi u komori u blizini mjerjenog uzorka i neovisno o izvoru mjeri mu otpor metodom četiri kontakta. Jedinica za kontrolu temperature pokazuje temperaturu dobivenu iz poznate temperaturne ovisnosti otpora poluvodiča.

**Table C-1. Comparison of Liquid Helium and Liquid Nitrogen**

PROPERTY	LIQUID HELIUM	LIQUID NITROGEN
Boiling Point @1 atm, in K	4.2	77
Thermal Conductivity (Gas), w/cm-K	0.083	0.013
Latent Heat of Vaporization, Btu/liter	2.4	152
Liquid Density, pounds/liter	0.275	0.78

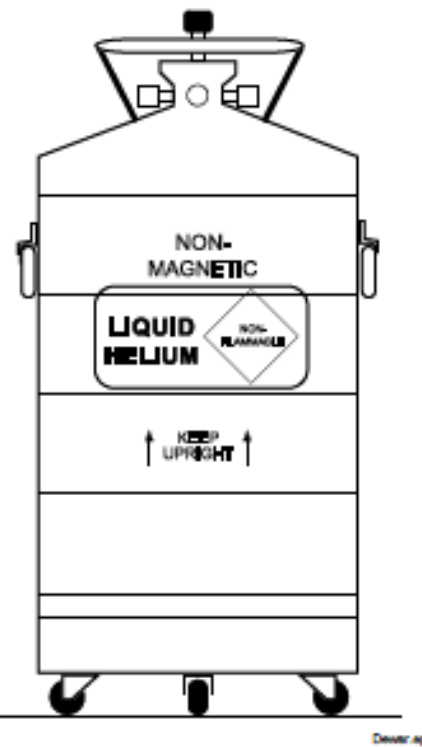


**Figure C-1. Typical Cryogenic Storage Dewar**

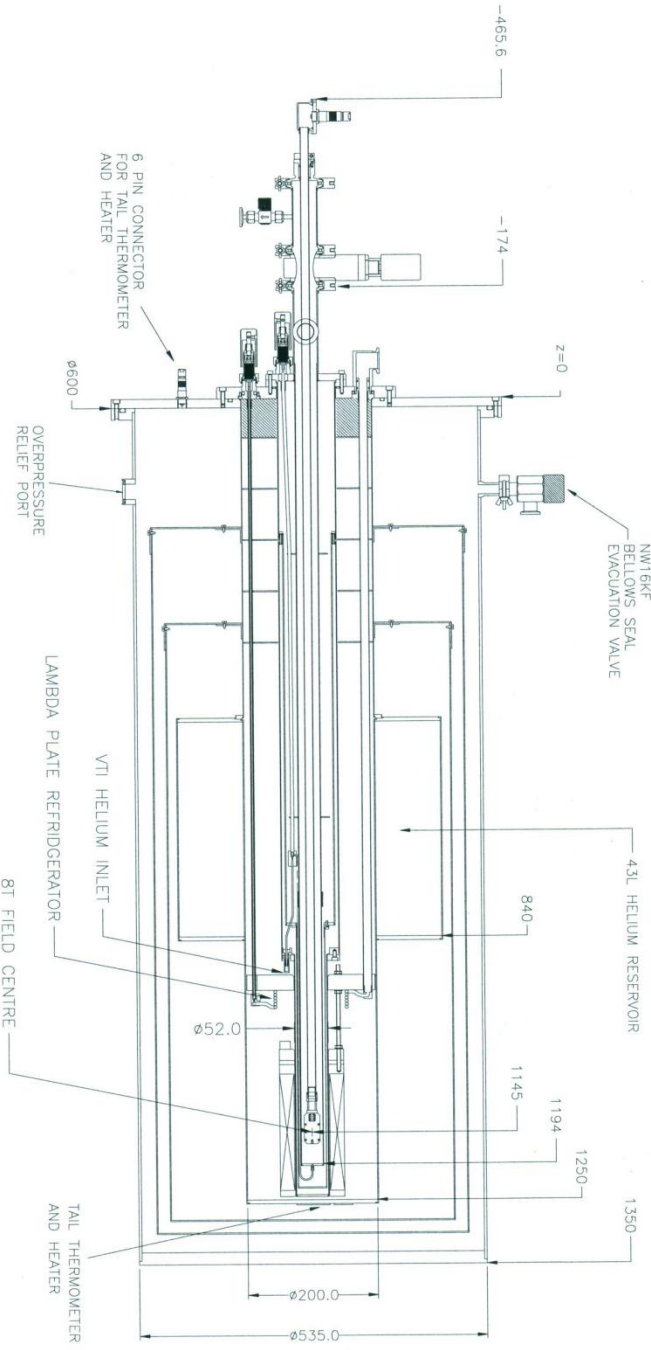
**Table B-2. Recommended SI Values for Physical Constants**

Quantity	Symbol	Value (SI units)
Permeability of Vacuum	$\mu_0$	$4\pi \times 10^{-7} \text{ H m}^{-1}$
Speed of Light in Vacuum	c	$2.9979 \times 10^8 \text{ m s}^{-1}$
Permittivity of Vacuum	$\epsilon_0 = (\mu_0 c^2)^{-1}$	$8.8542 \times 10^{-12} \text{ F m}^{-1}$
Fine Structure Constant, $\mu_0 c e^2 / 2\hbar$	$\alpha$ $\alpha^{-1}$	0.0073 137.0360
Elementary Charge	e	$1.6022 \times 10^{-19} \text{ C}$
Plank's Constant	$\hbar$ $\hbar = h/2\pi$	$6.6262 \times 10^{-34} \text{ J Hz}^{-1}$ $1.0546 \times 10^{-34} \text{ J s}$
Avogadro's Constant	$N_A$	$6.0220 \times 10^{23} \text{ mol}^{-1}$
Atomic Mass Unit	$1 \text{ u} = 10^{-3} \text{ kg mol}^{-1}/N_A$	$1.6605 \times 10^{-27} \text{ kg}$
Electron Rest Mass	$m_e$	$9.109 \times 10^{-31} \text{ kg}$ $5.4858 \times 10^{-4} \text{ u}$
Proton Rest Mass	$m_p$	$1.6726 \times 10^{-27} \text{ kg}$ $1.0073 \text{ u}$
Neutron Rest Mass	$m_n$	$1.6749 \times 10^{-27} \text{ kg}$ $1.0087 \text{ u}$
Magnetic Flux Quantum	$\phi = h/2e$ $h/e$	$2.0679 \times 10^{-15} \text{ Wb}$ $4.1357 \times 10^{-15} \text{ J Hz}^{-1} \text{ C}^{-1}$
Josephson Frequency-Voltage Ratio	$2e/h$	$483.5939 \text{ THz V}^{-1}$
Quantum of Circulation	$h/m_e$ $h/m_n$	$3.6369 \times 10^{-4} \text{ J Hz}^{-1} \text{ kg}^{-1}$ $7.2739 \times 10^{-4} \text{ J Hz}^{-1} \text{ C}^{-1}$
Rydberg Constant	R <sub>n</sub>	$1.0974 \times 10^7 \text{ m}^{-1}$
Proton Moment in Nuclear Magnetons	$\mu_p/\mu_N$	2.7928
Bohr Magneton	$\mu_B = eh/2m_e$	$9.2741 \times 10^{-24} \text{ J T}^{-1}$
Proton Gyromagnetic Ratio	$\gamma_p$	$2.6752 \times 10^6 \text{ s}^{-1} \text{ T}^{-1}$
Diamagnetic Shielding Factor, Spherical H <sub>2</sub> O Sample	$1 + \sigma(\text{H}_2\text{O})$	1.0000
Molar Mass Constant	R	$8.3144 \text{ J mol}^{-1} \text{ K}^{-1}$
Molar Volume, Ideal Gas (T <sub>0</sub> = 273.15K, p <sub>0</sub> = 1 atm)	V <sub>m</sub> = RT <sub>0</sub> /p <sub>0</sub>	0.0224 m <sup>3</sup> mol <sup>-1</sup>
Boltzman Constant	k = R/N <sub>A</sub>	$1.3807 \times 10^{-23} \text{ J K}^{-1}$
Stefan-Boltzman Constant	$\sigma = (\pi^2/60) k^4/h^3 c^2$	$5.6703 \times 10^{-8} \text{ W m}^{-2} \text{ K}^{-4}$
First Radiation Constant	c <sub>1</sub> = 2πhc <sup>2</sup>	$3.7418 \times 10^{-16} \text{ W m}^{-2}$
Second Radiation Constant	c <sub>2</sub> = hc/k	0.0144 mK
Gravitation Constant	G	$6.6720 \times 10^{-11} \text{ N m}^2 \text{ kg}^{-2}$

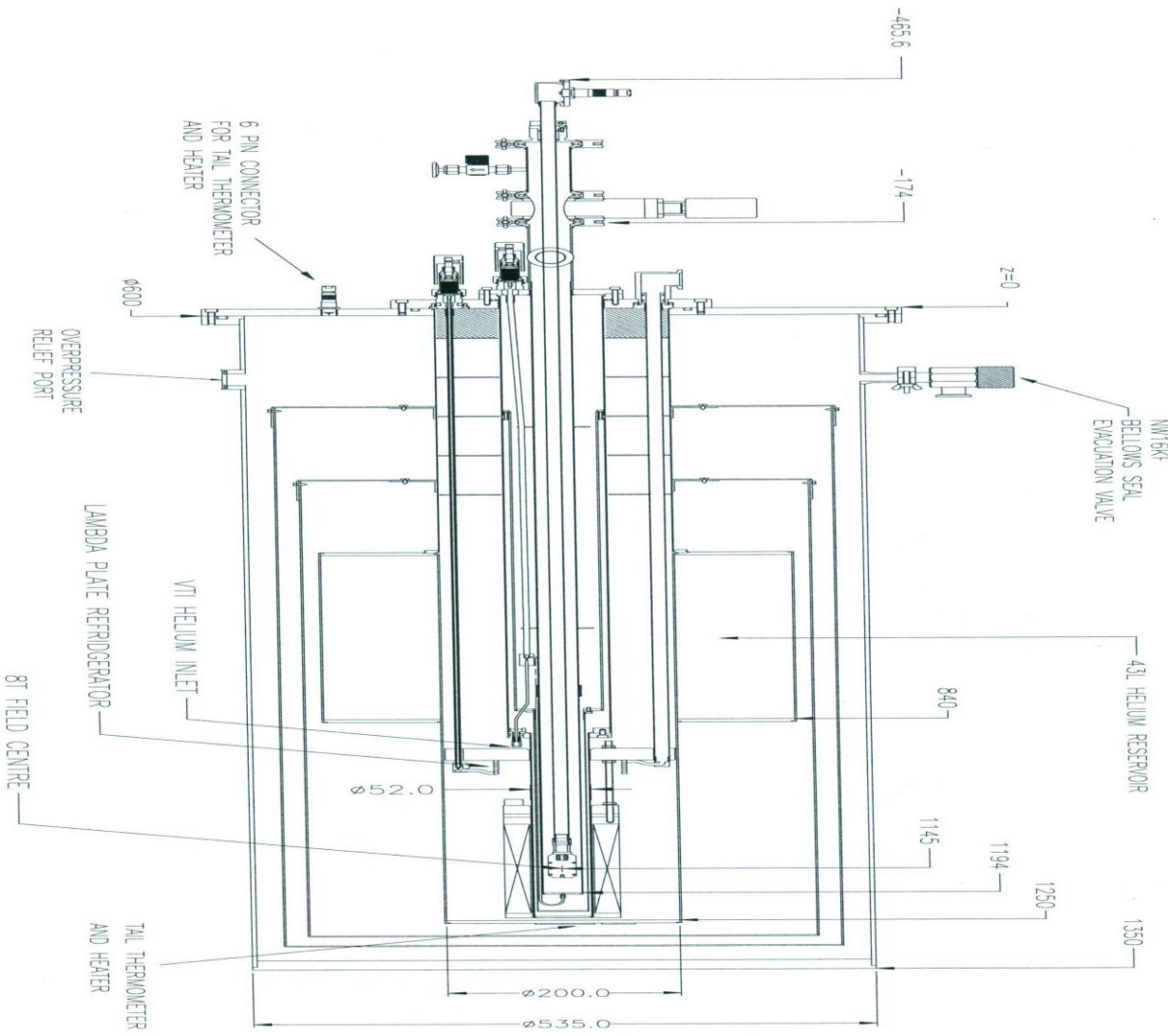
# He kriostat



# Kriostat



# Kriostat



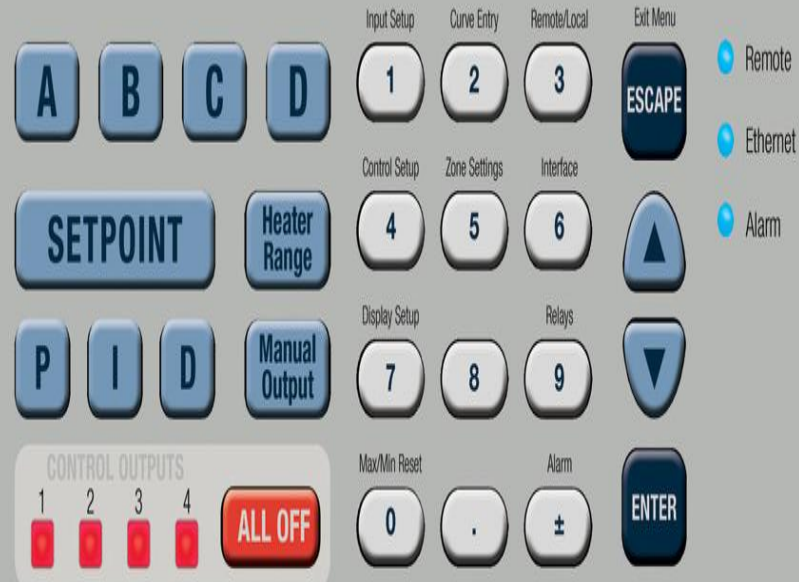
## Temperaturna kontrola

LakeShore

A: Input A      0.0000 K Max  
**367.096** K      0.0000 K Min  
 +0.35595 V

Ctrl Output: 1      P 50.0  
 Setp 376.000 K      I 20.0      MOut  
 Heat 0.00% of Off      D 0.0      0.00%

Model 350 Temperature Controller



A: Sample Space      B: Rad Shield  
**5.2014** K      27.8645 K  
 HI: 5.2000 K      LO: 0.0000 K      QC:  
 C: Heater      D: Monitor  
**4.6103**      35.6387 K  
 HI: 0.0000 K      LO: 0.0000 K      QC:

A: Sample Space      B: Rad Shield  
**5.2014** K      27.8645 K  
 HI: 5.2000 K      LO: 0.0000 K      QC:  
 L1: Sample Space      P: 50.0  
 Setp 273.000 K      I: 20.0      MOut  
 Heat 0.00% of Low      D: 0.0      0.00%

Input Settings: B: Rad Shield  
 Sensor: 100Ω RTD  
 Range: 2.5 Volt  
 Curve: None  
 Filter: On  
 Filter Points: 64  
 Filter Window: 1.5  
 Input Name: Rad Shield

FIGURE 1-2 Displays showing four loop mode, input display mode and custom display mode

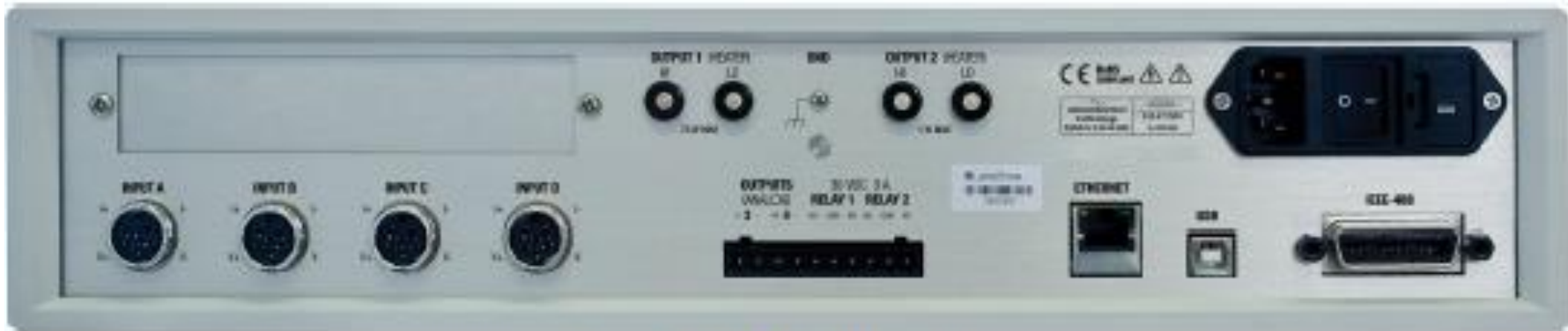


FIGURE 3-1 *Model 350 rear panel*

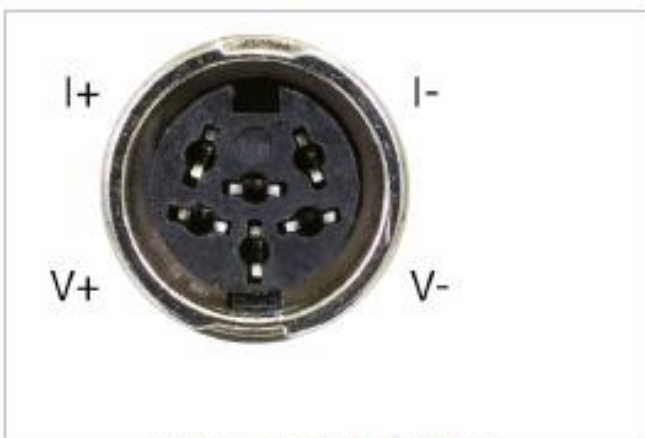


FIGURE 3-3 *Sensor input connector*

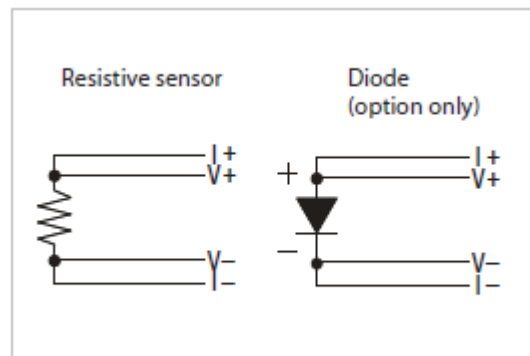


FIGURE 3-4 *4-lead measurement*

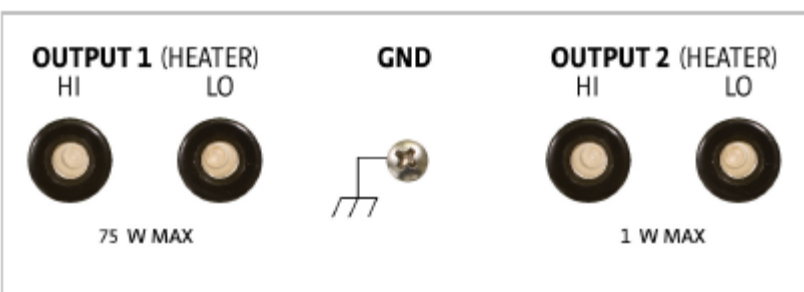


FIGURE 3-9 *Rear panel showing heater output connectors*

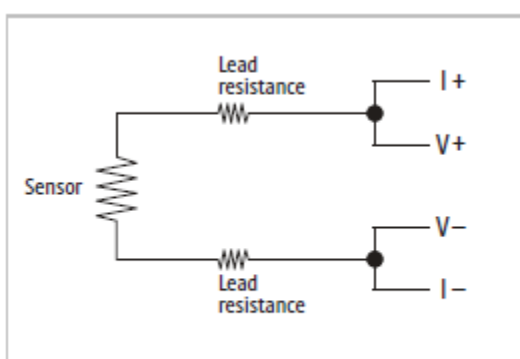


FIGURE 3-5 *2-lead sensor measurement*

		Model	Useful range	Magnetic field use
Negative Temperature Coefficient RTDs	Cernox™	OX-1010	0.1 K to 325 K <sup>1</sup>	T > 2 K & B ≤ 19 T
	Cernox™	OX-1030-HT	0.3 K to 420 K <sup>1</sup>	T > 2 K & B ≤ 19 T
	Cernox™	OX-1050-HT	1.4 K to 420 K <sup>1</sup>	T > 2 K & B ≤ 19 T
	Cernox™	OX-1070-HT	4 K to 420 K <sup>1</sup>	T > 2 K & B ≤ 19 T
	Cernox™	OX-1080-HT	20 K to 420 K <sup>1</sup>	T > 2 K & B ≤ 19 T
	Germanium	GR-300-AA	0.35 K to 100 K	Not recommended
	Germanium	GR-1400-AA	1.8 K to 100 K	Not recommended
	Rox™	RX-1028	0.1 K to 40 K	T > 2 K & B ≤ 10 T
	Rox™	RX-103	1.4 K to 40 K	T > 2 K & B ≤ 10 T
	Rox™	RX-202	0.5 K to 40 K	T > 2 K & B ≤ 10 T
Positive Temperature Coefficient RTDs	100 Ω platinum	PT-102/3	14 K to 873 K	T > 40 K & B ≤ 2.5 T
	100 Ω platinum	PT-111	14 K to 673 K	T > 40 K & B ≤ 2.5 T
	Rhodium-iron	RF-800-4	14 K to 500 K	T > 77 K & B ≤ 8 T
Diodes (3062)	Silicon Diode	DT-670-SD	1.4 K to 500 K	T ≥ 60 K & B ≤ 3 T
	Silicon Diode	DT-670E-BR	30 K to 500 K	T ≥ 60 K & B ≤ 3 T
	Silicon Diode	DT-414	1.4 K to 375 K	T ≥ 60 K & B ≤ 3 T
	Silicon Diode	DT-421	1.4 K to 325 K	T ≥ 60 K & B ≤ 3 T
	Silicon Diode	DT-470-SD	1.4 K to 500 K	T ≥ 60 K & B ≤ 3 T
	Silicon Diode	DT-471-SD	10 K to 500 K	T ≥ 60 K & B ≤ 3 T
	GaAlAs Diode	TG-120-P	1.4 K to 325 K	T > 4.2 K & B ≤ 5 T
	GaAlAs Diode	TG-120-PL	1.4 K to 325 K	T > 4.2 K & B ≤ 5 T
	GaAlAs Diode	TG-120-SD	1.4 K to 500 K	T > 4.2 K & B ≤ 5 T
Capacitance (3061)		CS-501	1.4 K to 290 K	T > 4.2 K & B ≤ 18.7 T
Thermocouples (3060)	Type K	9006-006	3.2 K to 1505 K	Not recommended
	Type E	9006-004	3.2 K to 934 K	Not recommended
	Chromel-AuFe 0.07%	9006-002	1.2 K to 610 K	Not recommended

<sup>1</sup>Non-HT version maximum temperature: 325 K

TABLE 1-1 Sensor temperature range (sensors sold separately)

	Example Lake Shore Sensor	Temperature (K)	Nominal Resistance/ Voltage	Typical Sensor Sensitivity <sup>2</sup>	Measurement Resolution: Temperature Equivalents	Electronic Accuracy: Temperature Equivalents	Temperature Accuracy Including Electronic Accuracy, CalCurve™ and Calibrated Sensor	Electronic Control Stability <sup>3</sup> : Temperature Equivalents
Cernox™ (1 mV)	CX-1010-SD with 0.1L calibration	0.1	21389 Ω	-558110 Ω/K	5.4 μK	±69 μK	±4.1 mK	±10.8 μK
		0.3	2322.4 Ω	-10785 Ω/K	28 μK	±272 μK	±4.3 mK	±55.6 μK
		0.5	1248.2 Ω	-2665.2 Ω/K	113 μK	±938 μK	±4.9 mK	±225 μK
		4.2	277.32 Ω	-32.209 Ω/K	931 μK	±6.5 mK	±11 mK	±190 μK
		300	30.392 Ω	-0.0654 Ω/K	153 mK	±1.7 K	±1.8 K	±306 mK
Cernox™ (10 mV)	CX-1050-SD-HT4 with 1.4M calibration	1.4	26566 Ω	-48449 Ω/K	6.2 μK	±261 μK	±4.3 mK	±12.4 μK
		4.2	3507.2 Ω	-1120.8 Ω/K	89 μK	±2.1 mK	±6.1 mK	±178 μK
		77	205.67 Ω	-2.4116 Ω/K	1.2 mK	±38 mK	±50 mK	±2.5 mK
		420	45.03Ω	-0.0829 Ω/K	12 mK	±338 mK	±412 mK	±24.1 mK
Germanium (1 mV)	GR-50-AA with 0.05A calibration	0.1	2317 Ω	-71858 Ω/K	4.2 μK	±21 μK	±4.0 mK	±8.3 μK
		0.3	164 Ω	-964 Ω/K	31.1 μK	±130 μK	±4.1 mK	±62.2 μK
		0.5	73.8 Ω	-202.9 Ω/K	49.3 μK	±244 μK	±4.2 mK	±98.6 μK
		1.4	24.7 Ω	-13.15 Ω/K	228 μK	±1.2 mK	±5.2 mK	±456 μK
		4.2	13.7 Ω	-1.036 Ω/K	2.9 mK	±11 mK	±15 mK	±5.8 mK
Germanium (10 mV)	GR-300-AA with 0.3D calibration	0.3	35180 Ω	-512200 Ω/K	2 μK	±47 μK	±4.0 mK	±3.9 μK
		1.4	448.6 Ω	-581.3 Ω/K	17 μK	±481 μK	±4.5 mK	±34.4 μK
		4.2	94.46 Ω	-26.56 Ω/K	38 μK	±1.8 mK	±5.8 mK	±75.3 μK
		100	2.72 Ω	-0.024 Ω/K	4.2 mK	±151 mK	±171 mK	±8.3 mK
Germanium (10 mV)	GR-1400-AA with 1.4D calibration	1.4	35890 Ω	-94790 Ω/K	11 μK	±257 μK	4.3 mK	±21.1 μK
		4.2	1689 Ω	-861.9 Ω/K	35 μK	±900 μK	4.9 mK	±69.6 μK
		77	3.55 Ω	-0.05 Ω/K	2 mK	±83 mK	94 mK	±4 mK
		100	2.8 Ω	-0.021 Ω/K	4.8 mK	±175 mK	195 mK	±9.5 mK
Rox™ (1 mV)	RX-102B-CB with 0.02C calibration	0.1	3549 Ω	-12578 Ω/K	79.5 μK	±908 μK	4.9 mK	±159 μK
		0.5	2188 Ω	-1056 Ω/K	284 μK	±2.7 mK	6.7 mK	±568 μK
		1.4	1779 Ω	-198 Ω/K	1.5 mK	±13.7 mK	18 mK	±3.0 mK
		4.2	1546 Ω	-40.0 Ω/K	7.5 mK	±65.4 mK	69 mK	±15.0 mK
		40	1199 Ω	-3.41 Ω/K	88 mK	±727 mK	803 mK	±176 mK
Platinum RTD 500 Ω Full Scale	PT-103 with 14J calibration	30	3.66 Ω	0.191 Ω/K	0.5 mK	±22 mK	±31 mK	±1.0 mK
		77	20.38 Ω	0.423 Ω/K	0.7 mK	±34 mK	±44 mK	±1.4 mK
		300	110.35 Ω	0.387 Ω/K	7.8 mK	±140 mK	±164 mK	±15.5 mK
		500	185.668 Ω	0.378 Ω/K	7.9 mK	±223 mK	±274 mK	±15.9 mK
Silicon Diode	DT-670-CO-13 with 1.4H calibration	1.4	1.664 V	-12.49 mV/K	0.8 mK	±13 mK	±20 mK	±1.6 mK
		77	1.028 V	-1.73 mV/K	5.8 mK	±76 mK	±113 mK	±11.6 mK
		300	0.5596 V	-2.3 mV/K	4.3 mK	±47 mK	±82 mK	±8.7 mK
		500	0.0907 V	-2.12 mV/K	4.7 mK	±40 mK	±94 mK	±9.4 mK
Silicon Diode	DT-470-SD-13 with 1.4H calibration	1.4	1.6981 V	-13.1 mV/K	0.8 mK	±13 mK	±20 mK	±1.5 mK
		77	1.0203 V	-1.92 mV/K	5.2 mK	±68 mK	±105 mK	±10.4 mK
		300	0.5189 V	-2.4 mV/K	4.2 mK	±44 mK	±79 mK	±8.3 mK
		475	0.0906 V	-2.22 mV/K	4.5 mK	±38 mK	±87 mK	±9.0 mK
GaAlAs Diode	TG-120-SD with 1.4H calibration	1.4	5.3909 V	-97.5 mV/K	0.21 mK	±6 mK	±13 mK	±410 μK
		77	1.4222 V	-1.24 mV/K	16 mK	±179 mK	±216 mK	±32.3 mK
		300	0.8978 V	-2.85 mV/K	7 mK	±60 mK	±95 mK	±14.0 mK
		475	0.3778 V	-3.15 mV/K	6.3 mK	±37 mK	±86 mK	±12.7 mK
Capacitance	CS-501	4.2	6.0 nF	27 pF/K	74 mK	NA	Calibration not available from Lake Shore	±14.8 mK
		77	9.1 nF	52 pF/K	39 mK			±7.7 mK
Thermocouple	Type K	200	19.2 nF	174 pF/K	12 mK			±23 mK
		75	-5862.9 μV	15.6 μV/K	26 mK	NA	Calibration not available from Lake Shore	±51.3 mK
		300	1075.3 μV	40.6 μV/K	9.9 mK			±19.7 mK
		600	13325 μV	41.7 μV/K	9.6 mK			±19.2 mK
		1500	49813 μV	36.1 μV/K	11 mK			±22.2 mK

<sup>2</sup> Typical sensor sensitivities were taken from representative calibrations for the sensor listed

<sup>3</sup> Control stability of the electronics only, in an ideal thermal system

<sup>4</sup> Non-HT version maximum temperature: 325 K

<sup>5</sup> Accuracy specification does not include errors from room temperature compensation

TABLE 1-2 Typical sensor performance

Sensor type	Temperature	Resistance typical, $R_e (\Omega)$	Sensitivity typical ( $\text{V}/(\text{K}\Omega)$ ) <sup>1</sup>	Thermal resistance typical, $R_t (\Omega)^2$	Excitation current (1 mV setting)	Typical self-heating $\Delta T_{SH} (\text{mK})^3$	Measurement resolution ( $\Omega$ ) <sup>4</sup>	Instrument noise ( $\mu\text{V}$ ) <sup>5</sup>	Instrument accuracy (gain & offset) <sup>6</sup>	Instrument accuracy ( $\text{mK})^7$	Sensor uncertainty ( $\text{mK})^8$	Total uncertainty = self-heating + (instrument + sensor) ( $\text{mK})^9$
RX-102B	100 mK	3,546	-12,578	$6 \times 10^7$	10 nA	+0.02	10	800	$\pm 100 \Omega$ (0.1%mg) $\pm 0.04\%$ rdg	$\pm 8.1$	$\pm 4$	$+0.0 \pm 12.1$
					30 nA	+0.2	3	240	$\pm 30 \Omega$ (0.1%mg) $\pm 0.04\%$ rdg	$\pm 2.5$		$+0.2 \pm 6.5$
					100 nA	+2.1	1	80	$\pm 10 \Omega$ (0.1%mg) $\pm 0.04\%$ rdg	$\pm 0.9$		$+2.1 \pm 4.9$
CR-50	100 mK	2,317	-71,858	$6 \times 10^7$	10 nA	+0.0	10	140	$\pm 100 \Omega$ (0.1%mg) $\pm 0.04\%$ rdg	$\pm 1.4$	$\pm 4$	$+0.0 \pm 5.4$
					30 nA	+0.1	3	42	$\pm 30 \Omega$ (0.1%mg) $\pm 0.04\%$ rdg	$\pm 0.4$		$+0.1 \pm 4.4$
					100 nA	+1.4	1	14	$\pm 10 \Omega$ (0.1%mg) $\pm 0.04\%$ rdg	$\pm 0.2$		$+1.4 \pm 4.2$
					300 nA	+12.5	0.3	4	$\pm 2 \Omega$ (0.07%mg) $\pm 0.04\%$ rdg	$\pm 0.0$		$+12.5 \pm 4$
CX-1010	100 mK	21,389	-558,110	$2 \times 10^9$	10 nA	+4.3	10	18	$\pm 100 \Omega$ (0.1%mg) $\pm 0.04\%$ rdg	$\pm 0.2$	$\pm 4$	$+4.3 \pm 4.2$
					30 nA	+38.5	3	6	$\pm 30 \Omega$ (0.1%mg) $\pm 0.04\%$ rdg	$\pm 0.1$		$+38.5 \pm 4.1$

1. Temperature Control Catalog, Appendix G: Sensor Temperature Response Data Tables

2. Temperature Control Catalog, Appendix E: Temperature Measurement System

3.  $T_{SH} = I^2 R_e R_t$ , Typical Self-Heating Error = Excitation Current<sup>2</sup> \* Sensor Resistance \* Thermal Resistance

4. Temperature Equivalent Noise = Instrument Measurement Resolution ÷ Sensitivity

5. TABLE 1-3: Input Specifications

6. Temperature Equivalent Instrument Accuracy = (Instrument Gain Accuracy + Instrument Offset Accuracy) ÷ Sensitivity

7. Temperature Control Catalog, Appendix D: Sensor Calibration Accuracies

8. Total Uncertainty = Instrument Accuracy + Sensor Uncertainty + Self-Heating Error

TABLE 2-1 Ultra-low temperature considerations

# PID Control

For closed-loop operation, the Model 350 temperature controller uses an algorithm called PID control. The control equation for the PID algorithm has three variable terms: proportional (P), integral (I), and derivative (D). See FIGURE 2-4. Changing these variables for best control of a system is called tuning. The PID equation in the Model 350 is:

$$\text{Heater Output} = P \left[ e + I \int (e) dt + D \frac{de}{dt} \right]$$

where the error (e) is defined as:  $e = \text{Setpoint} - \text{Feedback Reading}$ .

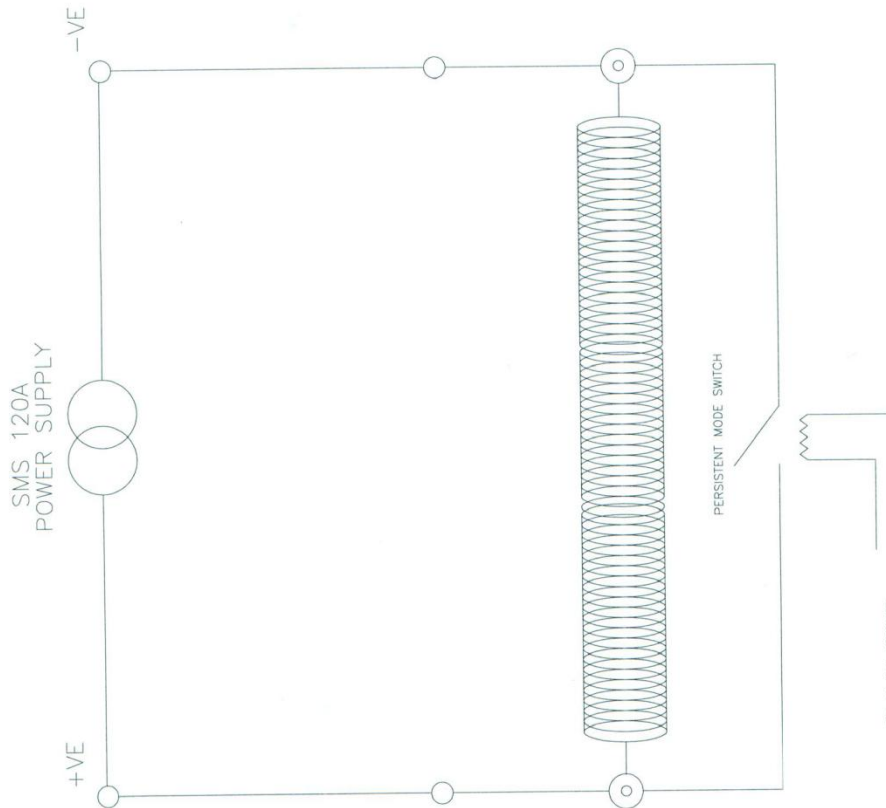
In the control loop, the integral term, also called reset, looks at error over time to build the integral contribution to the output:

$$\text{Output (I)} = PI \int (e) dt$$

The derivative term, also called rate, acts on the change in error with time to make its contribution to the output:

$$\text{Output (D)} = PD \frac{de}{dt}$$

# Supravodljivi magnet



# Model 625

## Superconducting Magnet Power Supply



- True 4-quadrant (bipolar) 60 A, 5 V output
- 0.1 mA output setting resolution
- Linear regulation minimizes noise and ripple to 0.006% of maximum current into a  $1\text{ m}\Omega$  load.
- 1.0 mA stability per hour
- Two units can be connected in parallel for  $\pm 120$  A operation



Figure 1-1. Model 625 Front Panel

## 1.2 SPECIFICATIONS

### Output

Type:	Bipolar, Four Quadrant, DC Current Source
Current Generation:	Linear regulation with digital setting and analog control
Current Range:	$\pm 60$ A
Compliance Voltage:	$\pm 5$ V maximum (nominal, both source and sink)
Maximum Power:	300 W
Load Reactance:	0 H to 100 H
Current Ripple (Max):	4 mA RMS at 60 A, (0.007%) into 1 m $\Omega$ load (significantly reduced into a reactive load or at lower current)
Current Ripple Frequency:	Dominated by line frequency and its harmonics
Temperature Coefficient:	$\pm 15$ ppm of full scale/ $^{\circ}$ C
Line Regulation:	15 ppm/6% line change
Source Impedance:	25 $\Omega$
Stability (1 h):	1 mA/h (after warm-up)
Stability (24 h):	10 mA/24 h (typical, dominated by temperature coefficient and line regulation)
Isolation:	Output optically isolated from chassis to prevent ground loops
Parallel Operation:	2 units can be paralleled for $\pm 120$ A, $\pm 5$ V operation
Protection:	Quench, Line Loss, Low Line Voltage, High Line Voltage, Output Over Voltage, Output Over Current, Over Temperature, Remote Inhibit (on critical error conditions, magnet discharges at 1 V nominal)

## Persistent Switch Heater Output (PSHO)

Current Range:	10 mA to 125 mA
Compliance Voltage (minimum):	12 V or 21 V selectable
Heater Resistance (minimum):	10 Ω
Setting Resolution:	1 mA
Accuracy:	±1 mA
Operation:	On/Off with lockout delay of 5 s to 100 s
Protection:	Open or shorted heater detection, error message if off and on output currents differ
Connector:	BNC

## Interface

### IEEE-488.2 Interface

Features:	SH1,AH1,T5,L4,SR1,RL1,PP0,DC1,DT1,C0,E1
Reading Rate:	To 10 readings/s
Software Support:	National Instruments LabVIEW driver (consult Lake Shore for availability)

### Serial Interface

Electrical Format:	RS-232C
Baud Rates:	9600, 19200, 38400, 57600
Reading Rate:	To 10 readings/s
Connector:	9-pin D-sub

### Output Current Monitor

Sensitivity:	60 A = 6 V
Accuracy:	±1% of full scale
Noise:	1 mV
Source Impedance:	20 Ω
Connector:	Shared 15-pin D-sub



Figure 2-1. Typical Superconducting Magnet

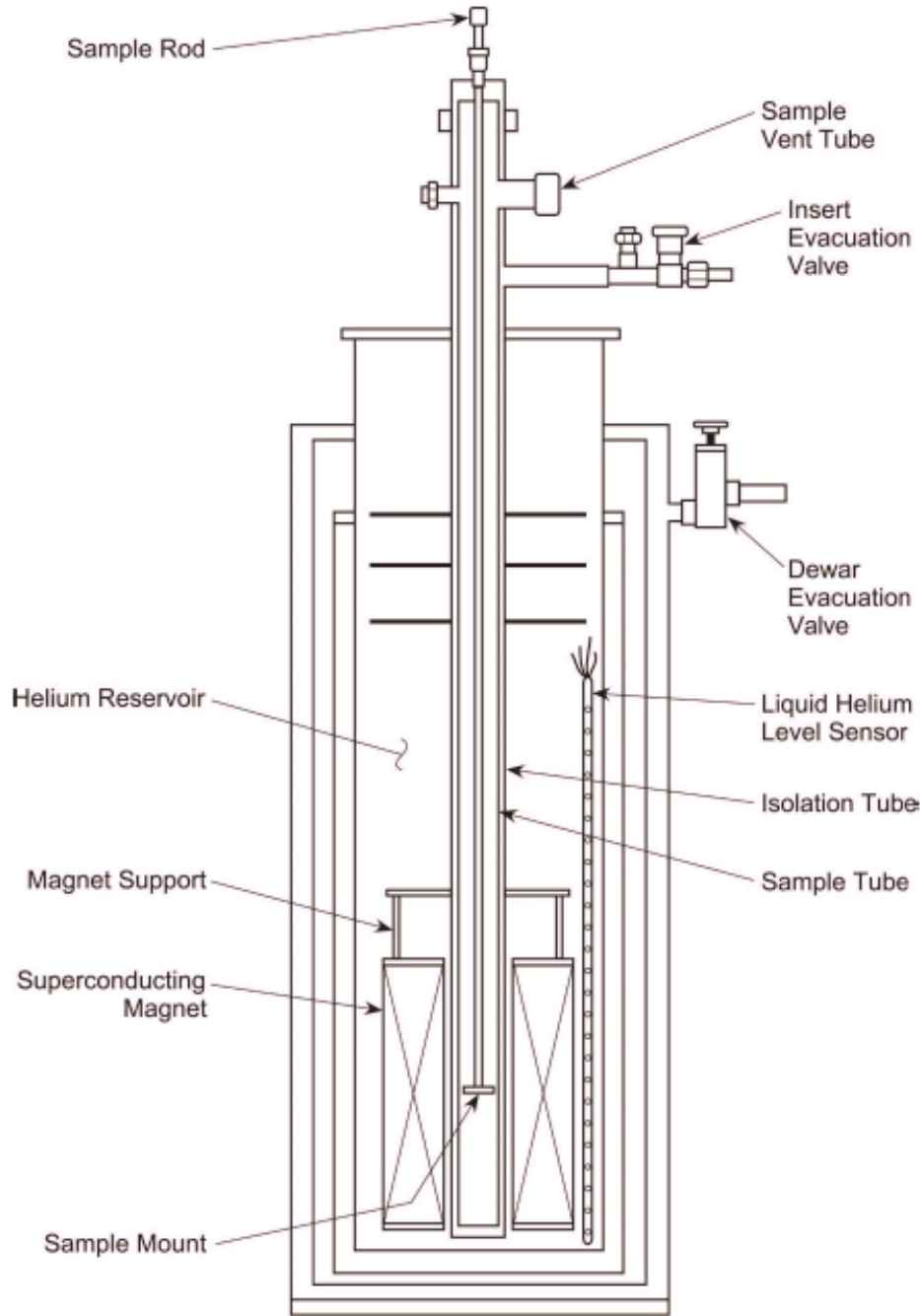


Figure 2-2. Cutaway of a Typical Helium Dewar, Magnet, and Insert

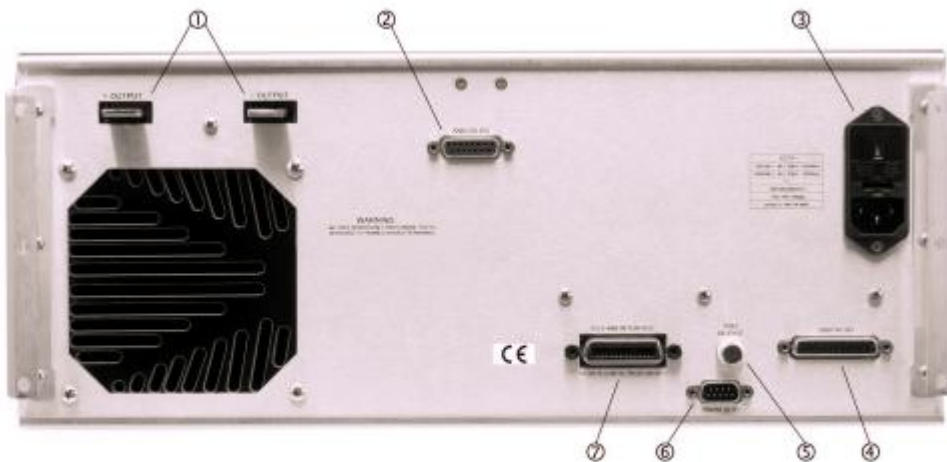
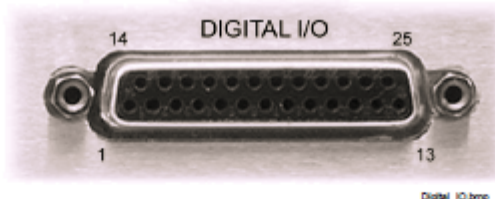


Figure 3-1. Model 625 Rear Panel



Digital\_I\_O.bmp

Pin	Name	Pin	Name
1	Fault Out Common	14	Fault Out
2	NC	15	NC
3	Remote Inhibit Common	16	Remote Inhibit
4	NC	17	NC
5	Trigger Out Common (not used)	18	Trigger Out (not used)
6	NC	19	NC
7	Trigger In Common	20	Trigger In
8	NC	21	NC
9	NC	22	NC
10	NC	23	NC
11	NC	24	NC
12	NC	25	NC
13	NC		

Figure 3-4. Model 625 Digital Input/Output Connector



Heater\_Output.bmp

Figure 3-6. Persistent Switch Heater Output Connector

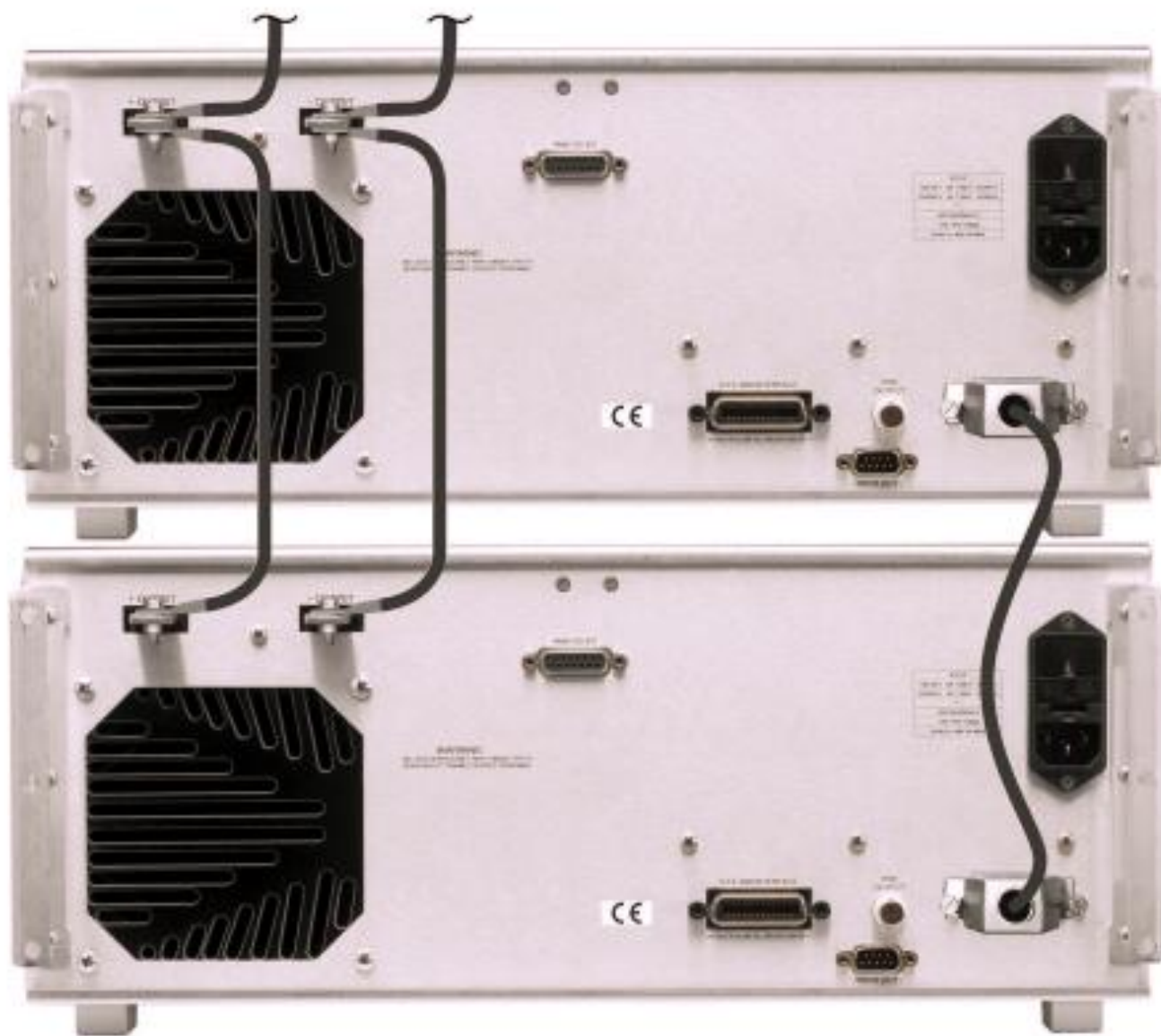


Figure 3-7. Connecting Two Power Supplies in Parallel

Output I	Output V
+60.0000 A	+0.1346 V
Set: +60.0000 A	V Limit: 5.0000 V
Rate: 0.1000 A/s	V Sense: +0.0085 V
PSH On: 40 mA	

Figure 4-1. Model 625 Output Current Display

Magnet Field	Output I: +60.0000 A
+8.50000 T	Set: +60.0000 A
Set: +8.50000 T	Output V: +0.1346 V
Rate: 0.1000 A/s	V Limit: 5.0000 V
	V Sense: +0.0085 V
	PSH On: 40 mA

Figure 4-2. Model 625 Magnet Field Display

Ramp Segments	
Current	Ramp Rate
1: 10.0000 A	1.0000 A/s
2: 15.0000 A	0.8000 A/s
3: 20.0000 A	0.7000 A/s
4: 30.0000 A	0.6000 A/s
5: 40.0000 A	0.5000 A/s

7651

PROGRAMMABLE DC SOURCE

+ .00000 mA

DATA

RMT

MODE  
RPT

SINGLE

CAL

OUT

TIME

PC

L

TIME

OUTPUT

V

+/-

1

2

3

4

5

CLR

RANGE

PRGM/END

STEP/^

mV

LOAD

I/F

DATA

INITIAL

SAVE

POWER

6

7

8

9

0

HOLD/DEL

RUN/▼

mA

SHIFT

LOCAL

ENTER

SRC

89438

GP-IB

Geeee488

address

02

Strujni izvori

WARNING △

GP-IB(IEEE488)

CAL SOURCE

EXT TRIG & OUTPUT △

MODEL 765111  
NO. 27D217244 B  
YOKOGAWA ◆ Made in Japan

48 - 63Hz 30W MAX

TERM

IN OUT GND OUT G

230VAC

200VAC

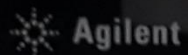
EXT TRIG & OUTPUT △

230VAC

GP-IB(IEEE488)

IEEE 488 GPIB

IEEE 488 GPIB



34420A  
7½ Digit Nano Volt / Micro Ohm Meter

0.000,91 mV Ch1

Max Measurement Level

Ch1: 120V

Ch2: 12V

350Vpk Max any terminal to  $\pm$

Power  
Scan  
Temp  
FUNCTION  
DCV1/DCV2  
DCV 1-2  
 $\Omega$  2W  
 $\Omega$  4W  
Chart Null  
Scale  
Filter Type  
Select Channel  
On/Off  
MENU Recall  
CHOICES  
LEVEL  
RANGE / DIGITS  
5  
6  
7  
ENTER  
Auto/Hold  
Auto/Man  
Single  
Shift  
LOCAL

Channel 1 DCV / Temp  
 $\Omega$  4W Source /  $\Omega$  2W  
HI LO  
Channel 2 DCV / Temp  
 $\Omega$  4W Sense  
HI



Nanovoltmeter

# Model 5210

## Dual Phase Lock-in Amplifier

### ***SIGNAL RECOVERY*** Model 5210

- Frequency range: 0.5 Hz to 120 kHz
- Voltage sensitivity: 100 nV to 3 V full-scale
- Current input mode sensitivities:
  - 10 fA to 300 nA full-scale
  - 10 fA to 3  $\mu$ A full-scale



- Line frequency rejection filter
- Dual phase demodulator with X-Y and R-θ outputs
- Fundamental (sine wave) or square-wave response modes
- Very low phase noise of < 0.005° rms.
- 3½-digit output readings
- Oscillator with variable amplitude and frequency
- Output time constants from 1 ms to 3 ks with 6 or 12 dB/octave roll-off
- Four external auxiliary ADC inputs
- One external DAC output
- Full range of auto-modes
- Standard GPIB (IEEE-488) and RS232 interfaces
- Two liquid crystal displays (LCD) and an analog panel meter for control and display of instrument outputs

# **Model 5210**

## **Dual Phase Lock-in Amplifier**



# Model 5210

## Dual Phase Lock-in Amplifier



Selected Voltage	Range (V rms)	Fuse Rating
100	80-110	1.0A
120	110-130	S.B.
220	210-230	0.5A
240	230-260	S.B.
48-62Vdc 120VA Maximum		250V

K-0604309



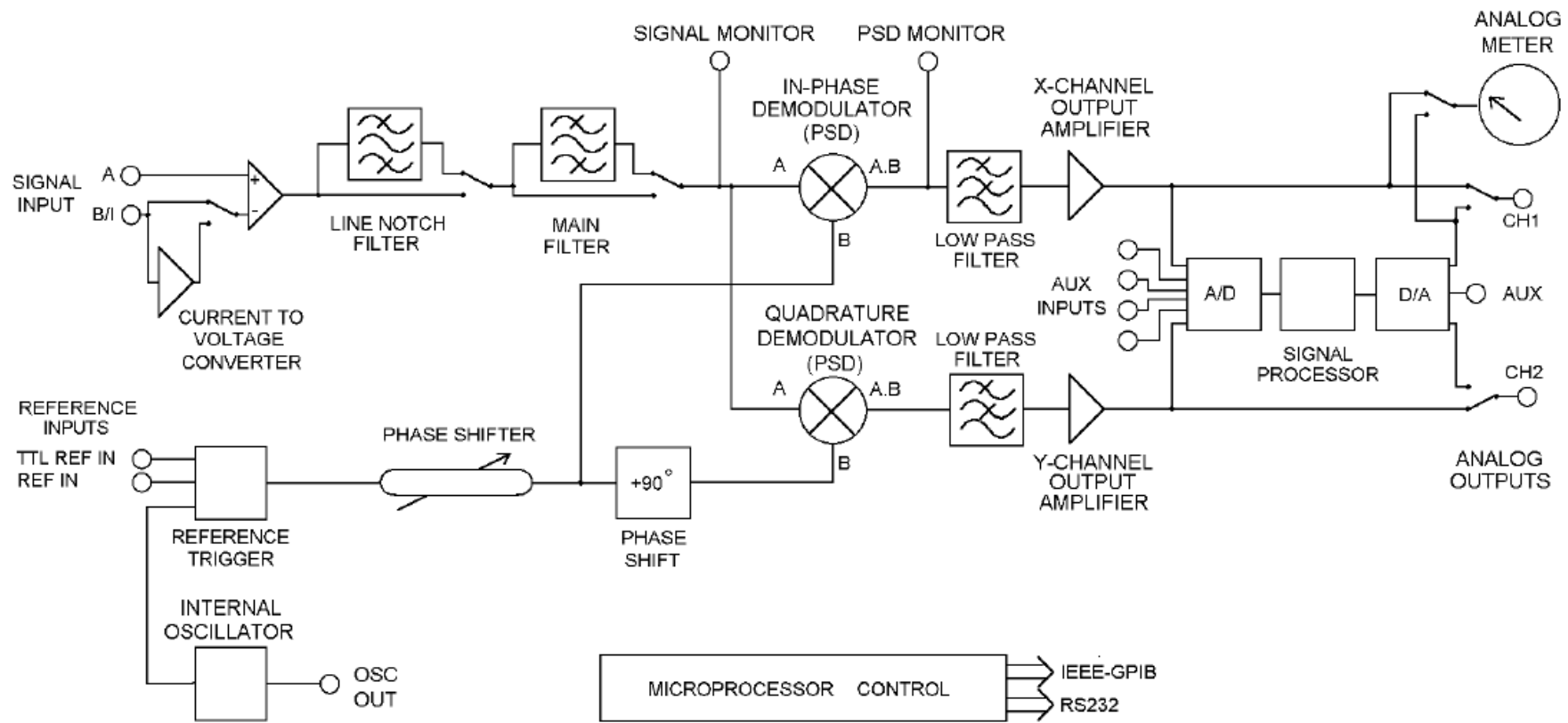


**Figure 3-1, Model 5210 - BLOCK DIAGRAM**

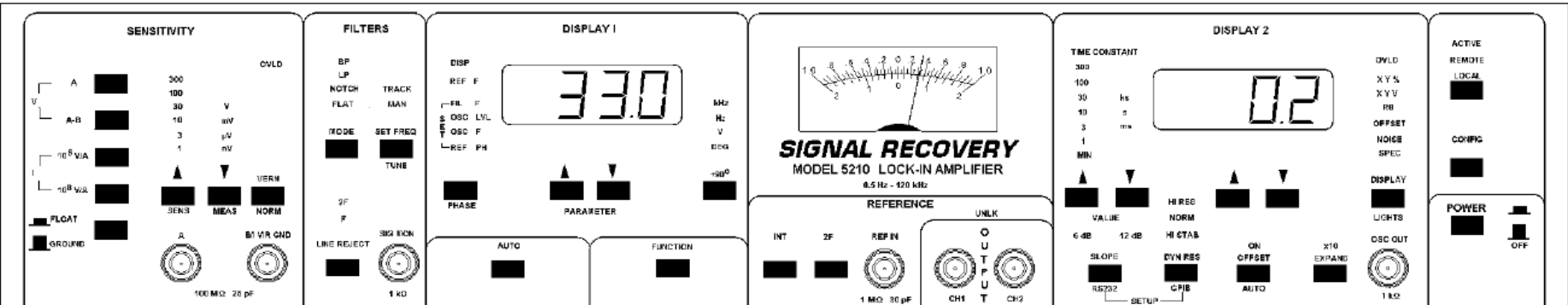


Figure 4-1, Model 5210 Front Panel Layout

Full-scale  
Sensitivity

3 V

1 V

300 mV

100 mV

30 mV

10 mV

3 mV

1 mV

300 µV

100 µV

30 µV

10 µV

3 µV

1 µV

300 nV

100 nV

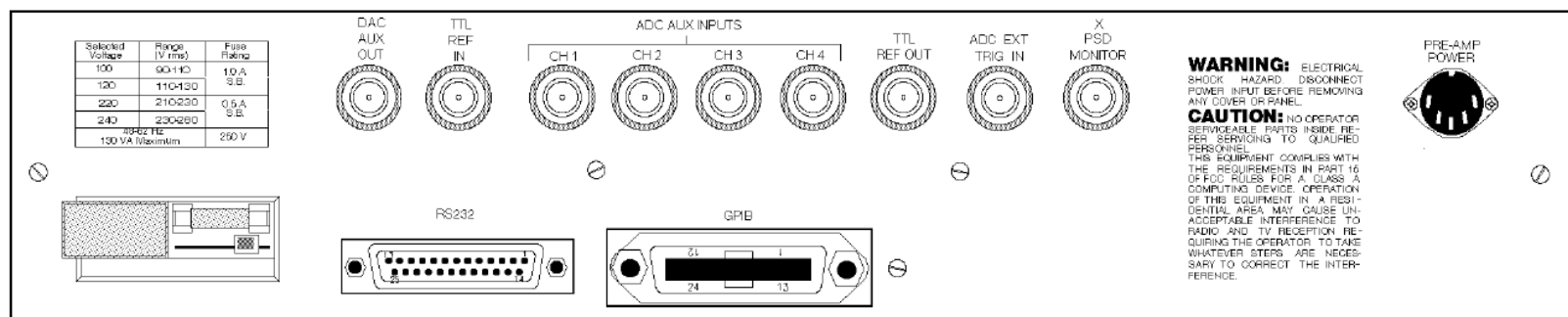
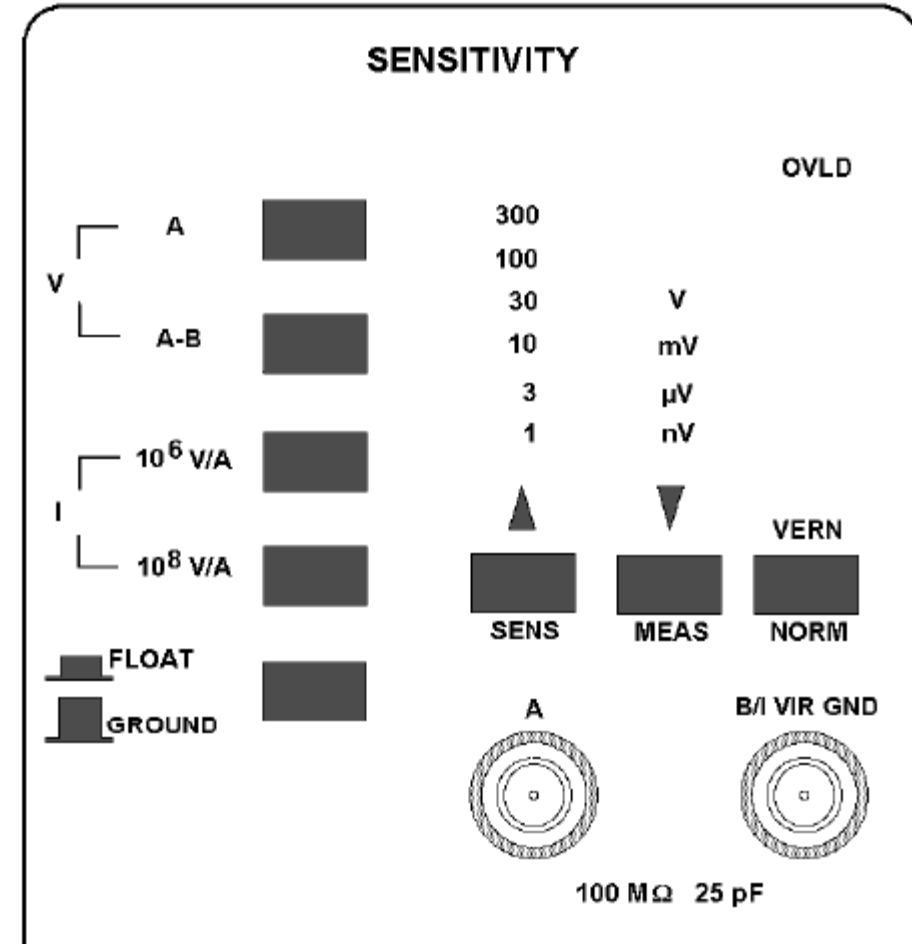


Figure 4-2, Model 5210 Rear Panel Layout



**Figure 5-1, SENSITIVITY Group**

## **Auto-Measure**

The secondary function of the **SENSITIVITY ▼** key is to initiate an auto-measure operation. Pressing the red **AUTO** key and then the **SENSITIVITY ▼** key will start this function, which consists of the following steps:

- 1) The red **AUTO** indicator lights.
- 2) The signal channel filter is set to the bandpass mode.
- 3) The signal channel filter frequency is tuned to the reference frequency by means of an auto-tune operation.
- 4) An auto-sensitivity operation is performed.
- 5) An auto-phase operation is performed.
- 6) The **AUTO** indicator extinguishes.

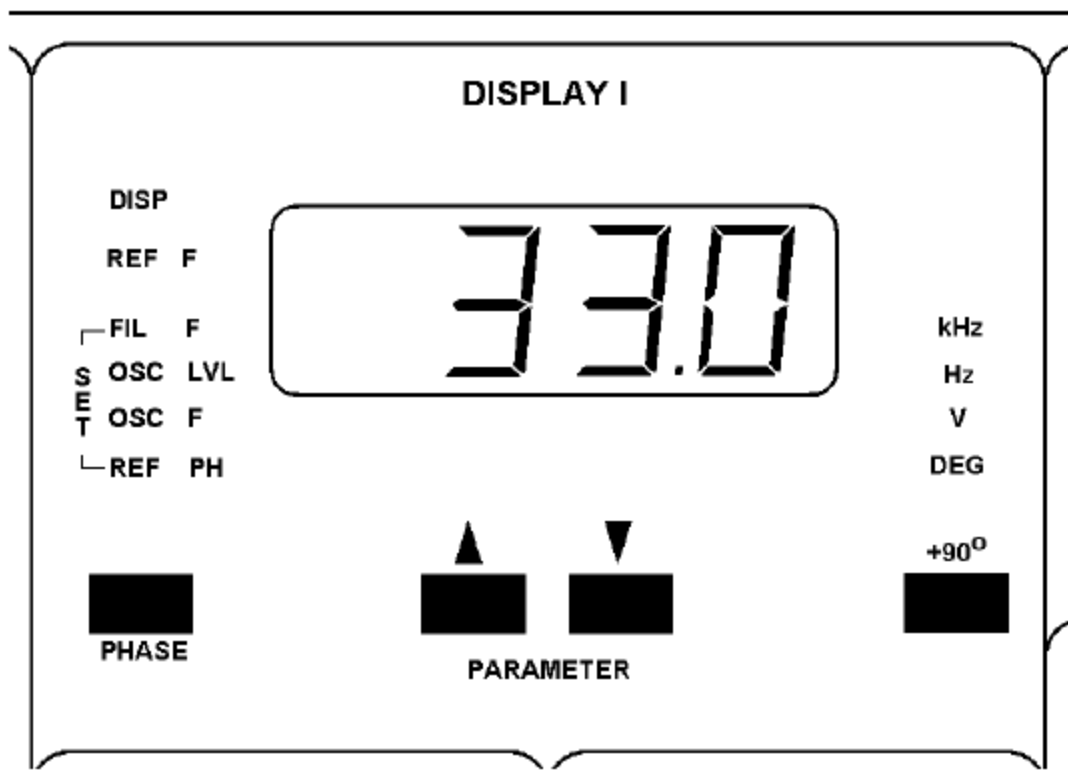
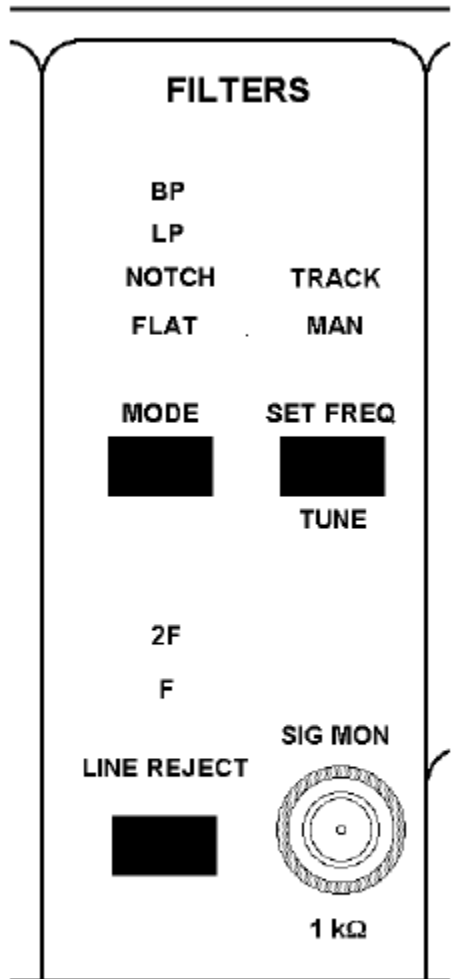


Figure 5-3, DISPLAY 1 Group

Figure 5-2, FILTERS Group

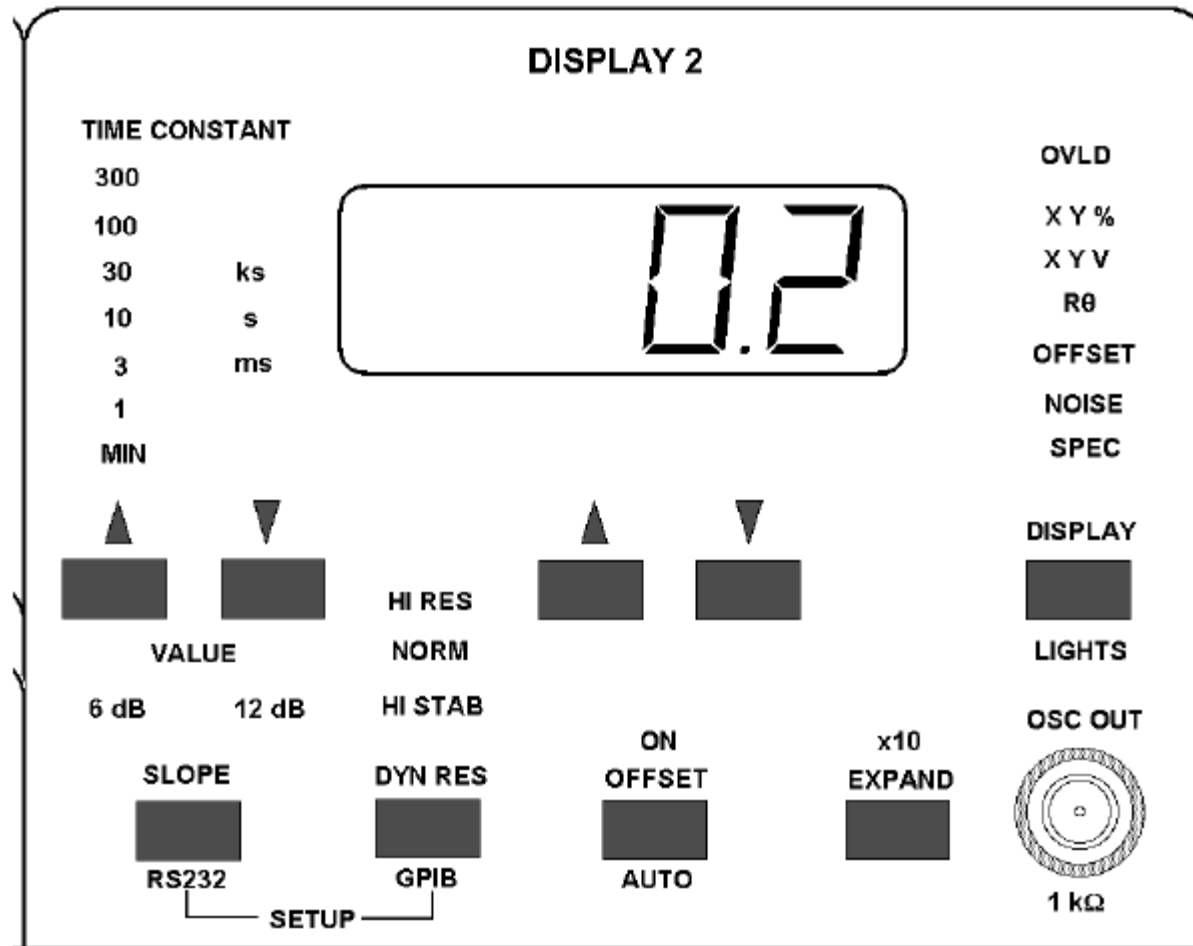
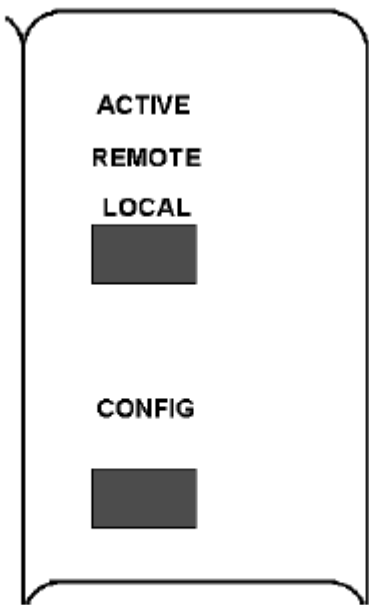


Figure 5-9, DISPLAY 2 Group



**Figure 5-10, Interface Group**

**Table C-1. Comparison of Liquid Helium and Liquid Nitrogen**

PROPERTY	LIQUID HELIUM	LIQUID NITROGEN
Boiling Point @1 atm, in K	4.2	77
Thermal Conductivity (Gas), w/cm-K	0.083	0.013
Latent Heat of Vaporization, Btu/liter	2.4	152
Liquid Density, pounds/liter	0.275	0.78

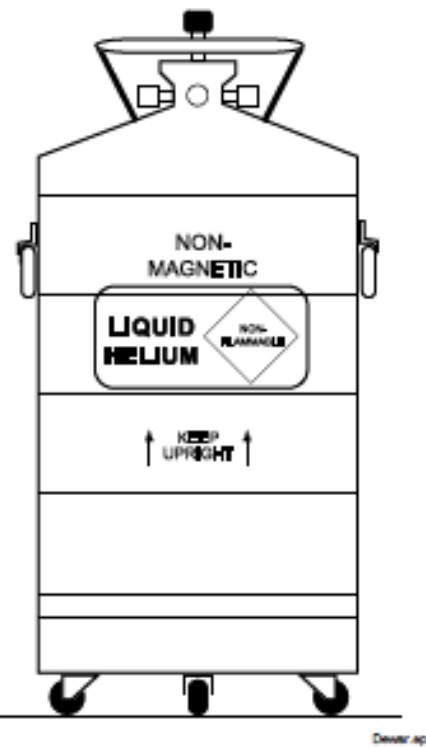
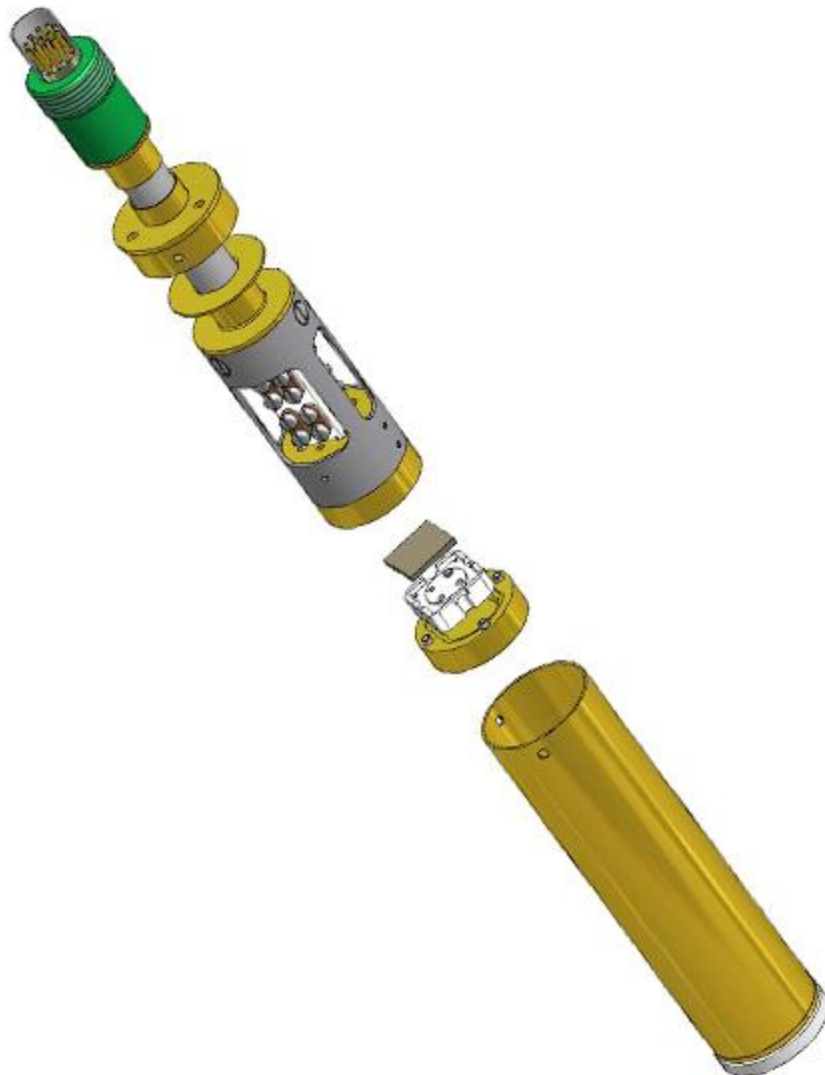


**Figure C-1. Typical Cryogenic Storage Dewar**

**Table B-2. Recommended SI Values for Physical Constants**

Quantity	Symbol	Value (SI units)
Permeability of Vacuum	$\mu_0$	$4\pi \times 10^{-7} \text{ H m}^{-1}$
Speed of Light in Vacuum	c	$2.9979 \times 10^8 \text{ m s}^{-1}$
Permittivity of Vacuum	$\epsilon_0 = (\mu_0 c^2)^{-1}$	$8.8542 \times 10^{-12} \text{ F m}^{-1}$
Fine Structure Constant, $\mu_0 c e^2 / 2\hbar$	$\alpha$ $\alpha^{-1}$	0.0073 137.0360
Elementary Charge	e	$1.6022 \times 10^{-19} \text{ C}$
Plank's Constant	$\hbar$ $\hbar = h/2\pi$	$6.6262 \times 10^{-34} \text{ J Hz}^{-1}$ $1.0546 \times 10^{-34} \text{ J s}$
Avogadro's Constant	N <sub>A</sub>	$6.0220 \times 10^{23} \text{ mol}^{-1}$
Atomic Mass Unit	1 u = $10^{-3} \text{ kg mol}^{-1}/N_A$	$1.6605 \times 10^{-27} \text{ kg}$
Electron Rest Mass	m <sub>e</sub>	$9.109 \times 10^{-31} \text{ kg}$ $5.4858 \times 10^{-4} \text{ u}$
Proton Rest Mass	m <sub>p</sub>	$1.6726 \times 10^{-27} \text{ kg}$ $1.0073 \text{ u}$
Neutron Rest Mass	m <sub>n</sub>	$1.6749 \times 10^{-27} \text{ kg}$ $1.0087 \text{ u}$
Magnetic Flux Quantum	$\phi = h/2e$ $h/e$	$2.0679 \times 10^{-15} \text{ Wb}$ $4.1357 \times 10^{-15} \text{ J Hz}^{-1} \text{ C}^{-1}$
Josephson Frequency-Voltage Ratio	2e/h	483.5939 THz V <sup>-1</sup>
Quantum of Circulation	$h/m_e$ $h/m_n$	$3.6369 \times 10^{-4} \text{ J Hz}^{-1} \text{ kg}^{-1}$ $7.2739 \times 10^{-4} \text{ J Hz}^{-1} \text{ C}^{-1}$
Rydberg Constant	R <sub>n</sub>	$1.0974 \times 10^7 \text{ m}^{-1}$
Proton Moment in Nuclear Magnetons	$\mu_p/\mu_N$	2.7928
Bohr Magneton	$\mu_B = eh/2m_e$	$9.2741 \times 10^{-24} \text{ J T}^{-1}$
Proton Gyromagnetic Ratio	$\gamma_p$	$2.6752 \times 10^6 \text{ s}^{-1} \text{ T}^{-1}$
Diamagnetic Shielding Factor, Spherical H <sub>2</sub> O Sample	1 + σ(H <sub>2</sub> O)	1.0000
Molar Mass Constant	R	$8.3144 \text{ J mol}^{-1} \text{ K}^{-1}$
Molar Volume, Ideal Gas (T <sub>0</sub> = 273.15K, p <sub>0</sub> = 1 atm)	V <sub>m</sub> = RT <sub>0</sub> /p <sub>0</sub>	0.0224 m <sup>3</sup> mol <sup>-1</sup>
Boltzman Constant	k = R/N <sub>A</sub>	$1.3807 \times 10^{-23} \text{ J K}^{-1}$
Stefan-Boltzman Constant	$\sigma = (\pi^2/60) k^4/h^3 c^2$	$5.6703 \times 10^{-8} \text{ W m}^{-2} \text{ K}^{-4}$
First Radiation Constant	c <sub>1</sub> = $2\pi hc^2$	$3.7418 \times 10^{-16} \text{ W m}^{-2}$
Second Radiation Constant	c <sub>2</sub> = $hc/k$	0.0144 mK
Gravitation Constant	G	$6.6720 \times 10^{-11} \text{ N m}^2 \text{ kg}^{-2}$



Nosač uzoraka

Nosač uzorka za mjerjenje anizotropnih svojstava uzorka



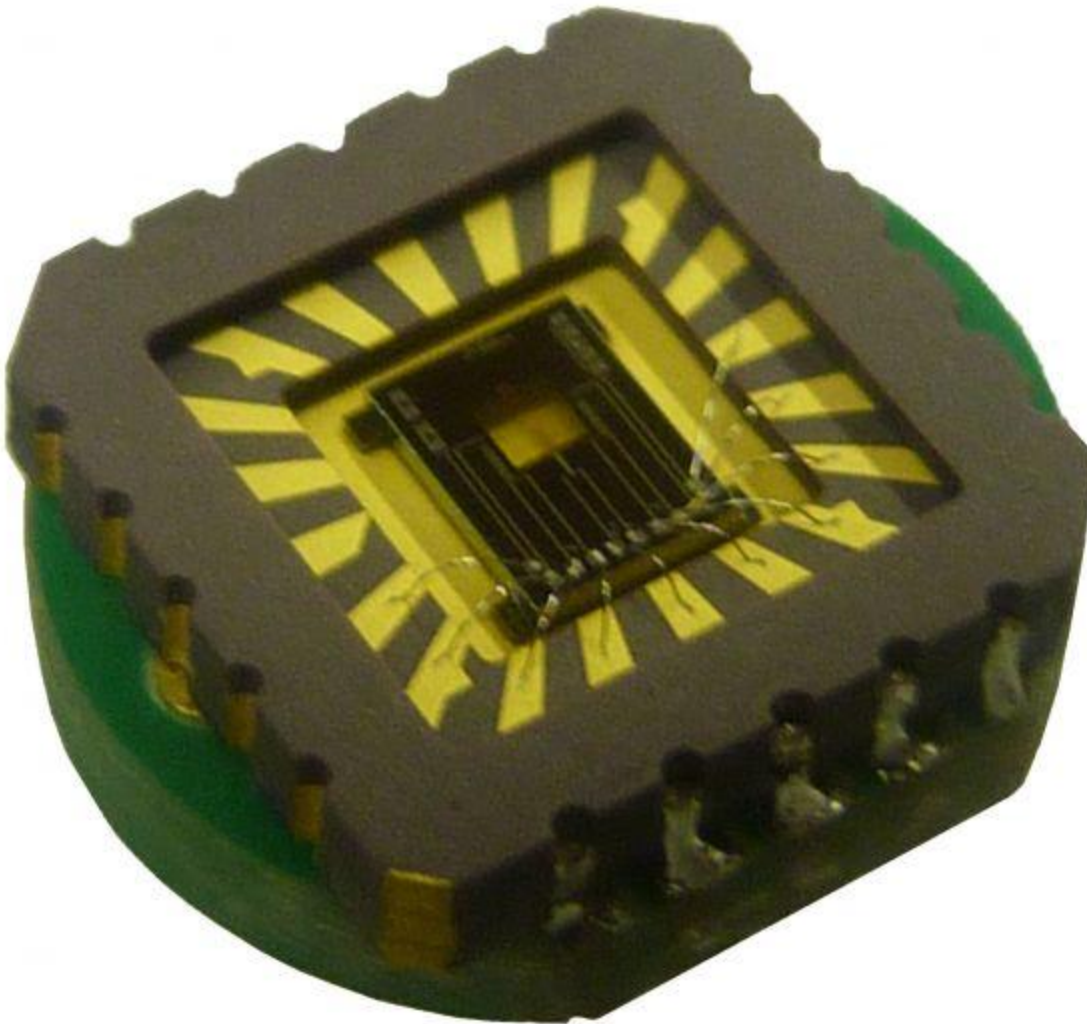
Nosač uzorka za mjerjenje anizotropnih svojstava uzorka



## Nosač uzorka za mjerjenje toplinske vodljivosti



Nosač uzorka za mjerjenje toplinskog kapaciteta

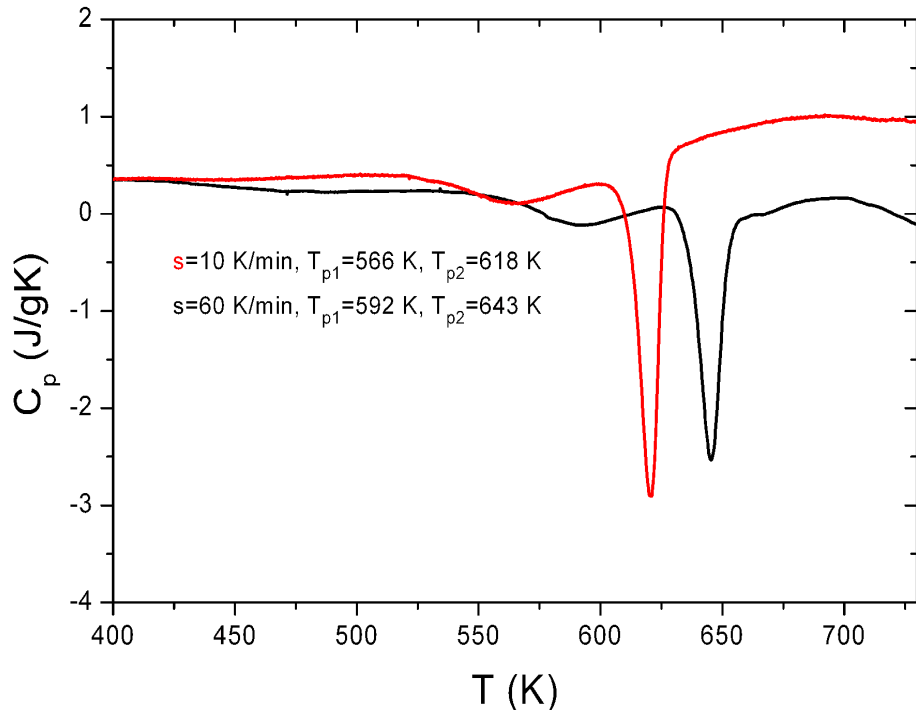


# Rezultati

## DSC i x-ray mjerena

- $\text{Zr}_{80}\text{Ni}_{20}$  uzorci su grijani brzinom 10 ili 60 K/min
- Javlja se oštar egzoterm iznad 600 K, na većoj temperaturi za uzorak grijan većom brzinom
- Blaži egzoterm uočljiv je na nižoj temperaturi, posljedica izlučivanja  $\omega$ -Zr faze
- Prema Kissingerovom modelu temperature ta dva egzoterma povezane su relacijom:

$$s = AT_{p1,p2}^2 \exp \left[ -\frac{E_{ai}}{k_B T_{p1,p2}} \right]$$



Toplinski tok  $c_p$  uzorka  $\text{Zr}_{80}\text{Ni}_{20}$  metalnog stakla pri aniliranju

- Aktivacijske energije uzorka su:

$$E_{a1} = (2.0 \pm 0.1) \text{ eV}$$

$$E_{a2} = (2.4 \pm 0.1) \text{ eV}$$

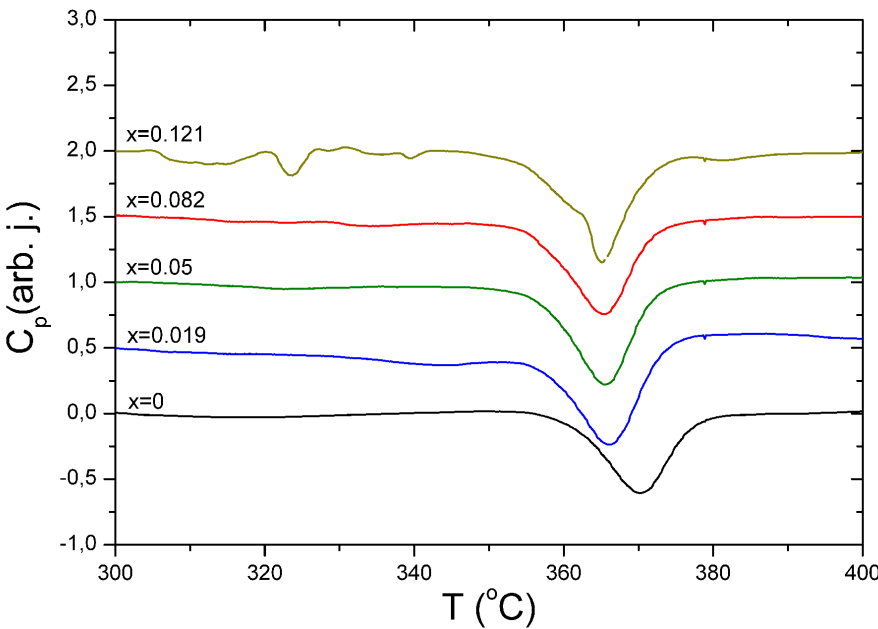
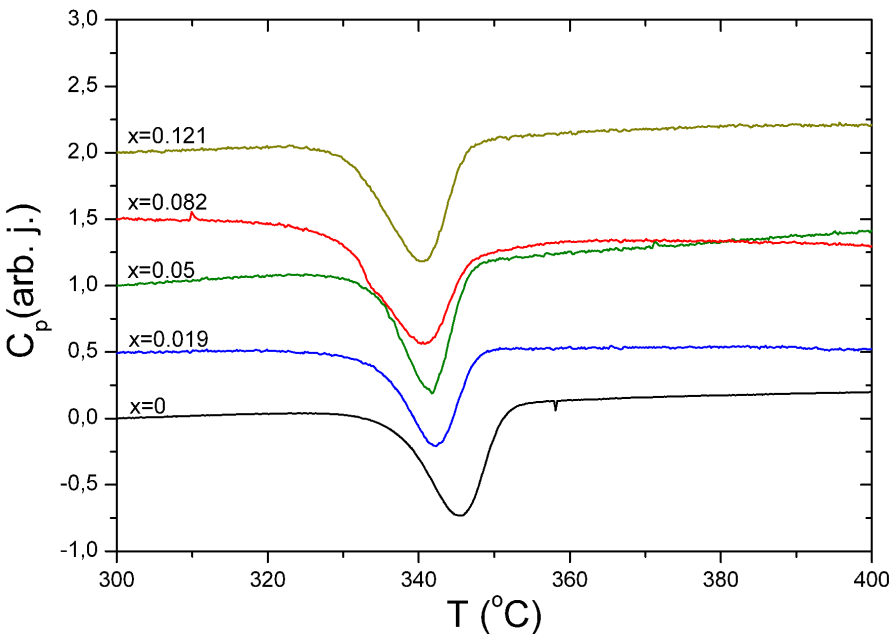
- Za određivanje energija se koriste rezultati više brzina grijanja

## Utjecaj vodika na stabilnost:

10 K/min

- Povećanje koncentracije vodika smanjuje temperaturu egzoterma
- Ovisnost je jača za manju koncentraciju vodika ( $x_H$ )
- Slična ovisnost kod grijanja brzinom 10 K/min i 60 K/min
- Uvođenjem vodika ekspandira amorfna struktura, povećava se difuzivnost pa se atomi lakše pomiču prema stabilnijim konfiguracijama
- Time se smanjuje  $E_a$  i  $T_p$
- Viša temperatura egzoterma za veću brzinu grijanja
- Proces je aniliranja se pokazao kao ireverzibilan

60 K/min



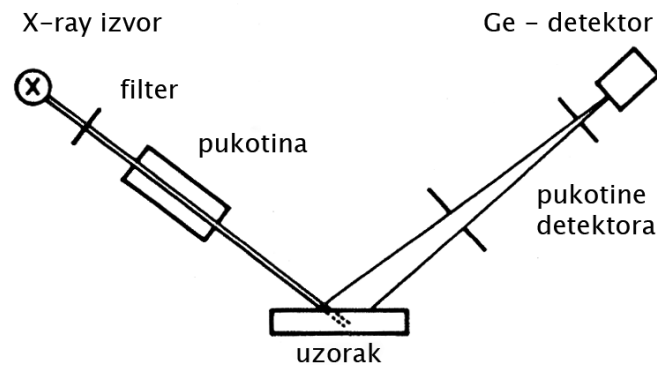
# X-ray rezultati

- Braggov zakon daje ovisnost položaja maksimuma o udaljenosti između centara raspršenja

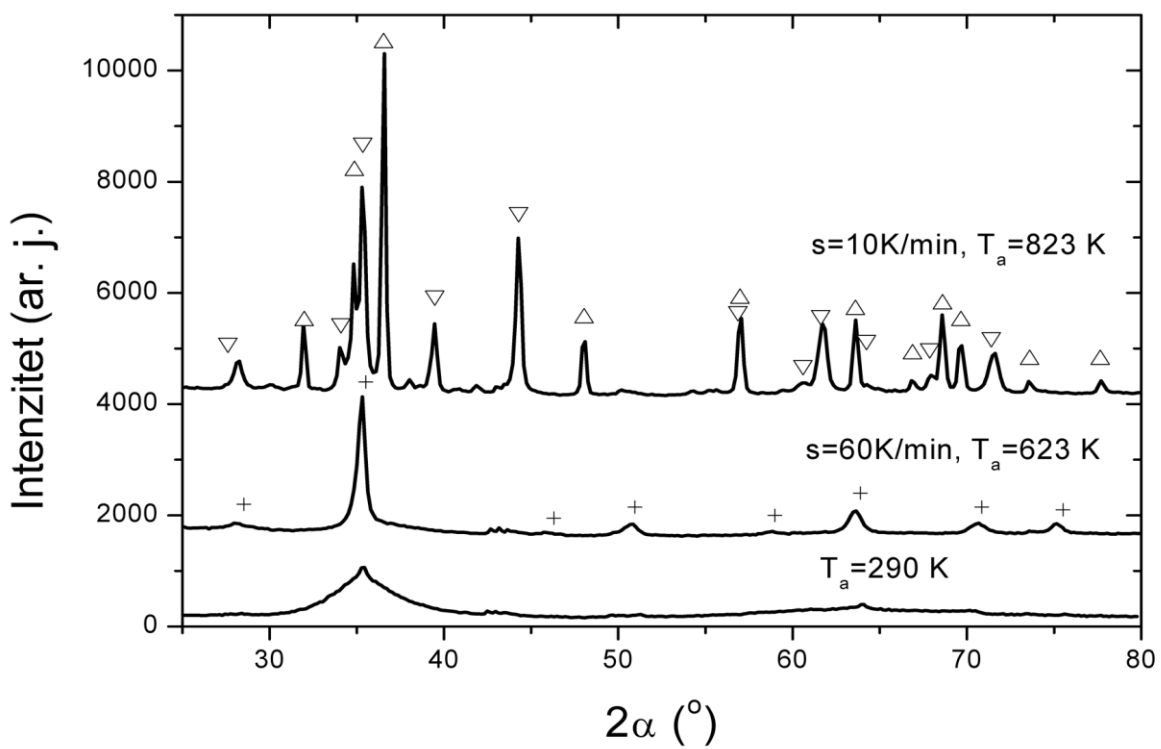
$$2d \sin(\theta) = n\lambda$$

- Korištenjem širine maksimuma na polovici širine  $\Delta\beta$ , položaja maksimuma  $\alpha$  i valne duljine  $\lambda$ , pomoću Scherrerove formule računa se veličina kristala

$$D = 0.9\lambda/(\Delta\beta \cos \alpha)$$

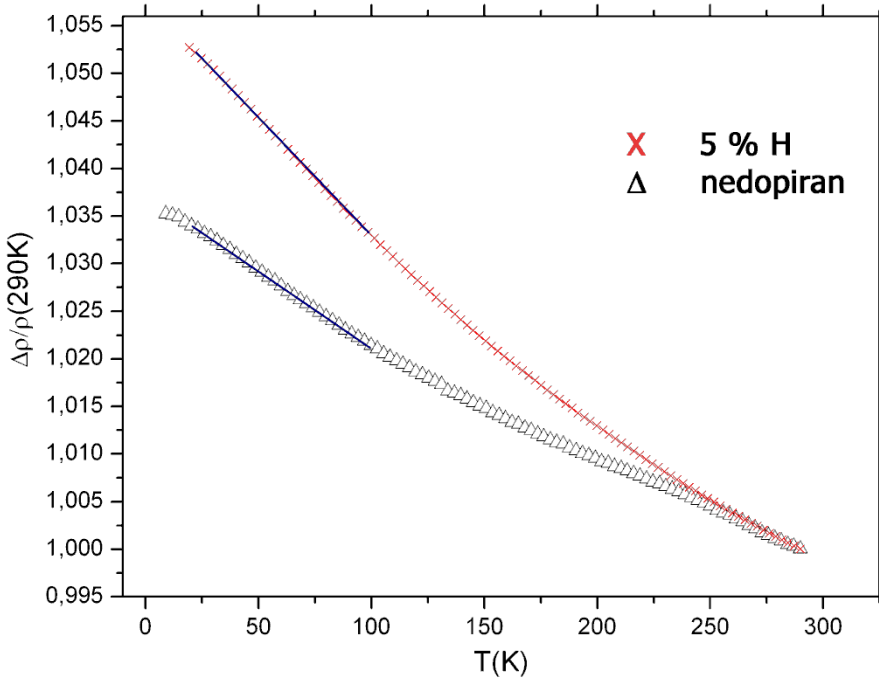


- Amorfni uzorak daje širok maksimum, ne javljuju se maksimumi kristalnih struktura
- Uzorak grijan brzinom  $60 \text{ K/min}$  do  $623 \text{ K}$  sadrži vrhove koji su prilagođeni  $\omega\text{-Zr}$  rešetci koja koegzistira s amorfnom matricom
- Uzorak grijan brzinom  $10 \text{ K/min}$  do  $823 \text{ K}$  pokazuje prisustvo kristala  $\text{Zr}_2\text{Ni}$  i  $\alpha\text{-Zr}$ , došlo je do drugog stupnja kristalizacije



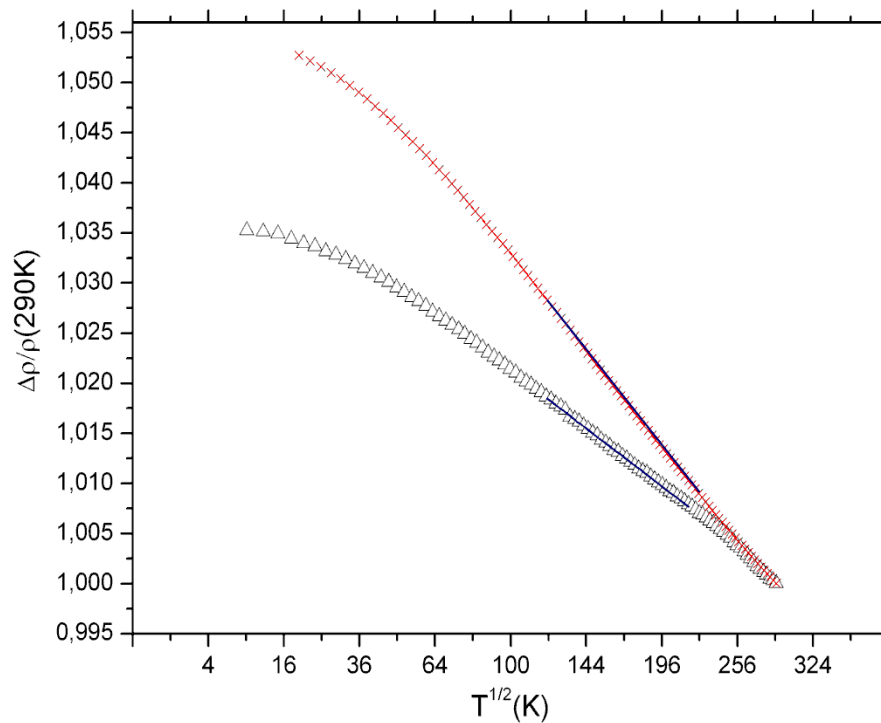
- Staklasti uzorak:  $2\alpha=35.9$
- $S=60 \text{ K/min}$   $\Delta\beta=3.7$
- $2\alpha=35.9$   $D=2.3 \text{ nm}$
- $\Delta\beta=3.7$   $\omega\text{-Zr}$
- $D=2.3 \text{ nm}$   $(P6/mmm)$
- $S=10 \text{ K/min}$  :  $2\alpha_1=35.35$   $\Delta\beta_1=0.4$
- $D_1=20.9 \text{ nm}$
- $\text{Zr}_2\text{Ni} (I4/mcm)$
- $2\alpha_2=36.43$   $\Delta\beta_2=0.35$
- $D_2=23.9 \text{ nm}$
- $\alpha\text{-Zr} (P6_3/mmc)$

# Otpornost staklastih uzoraka



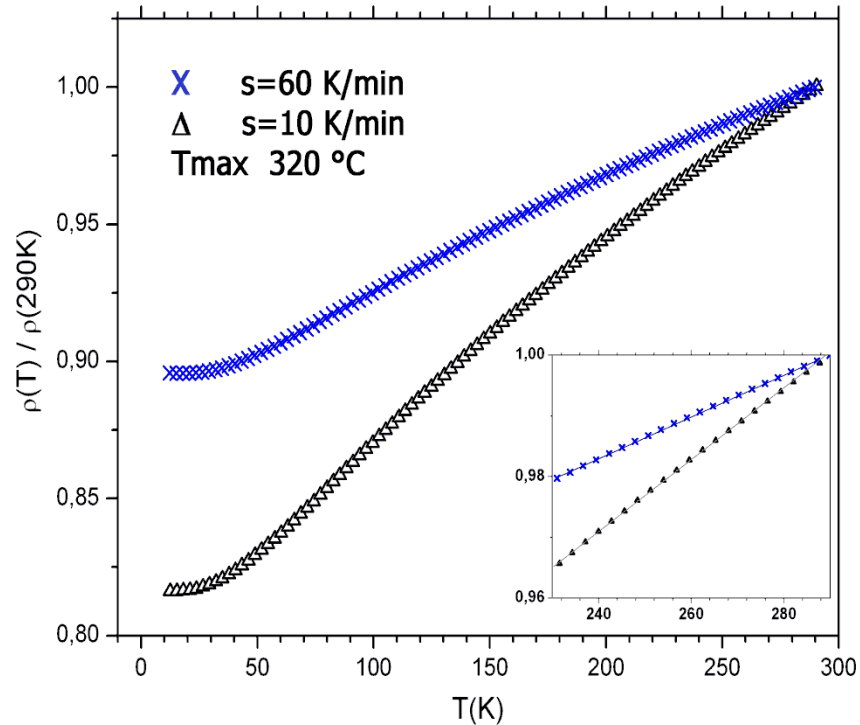
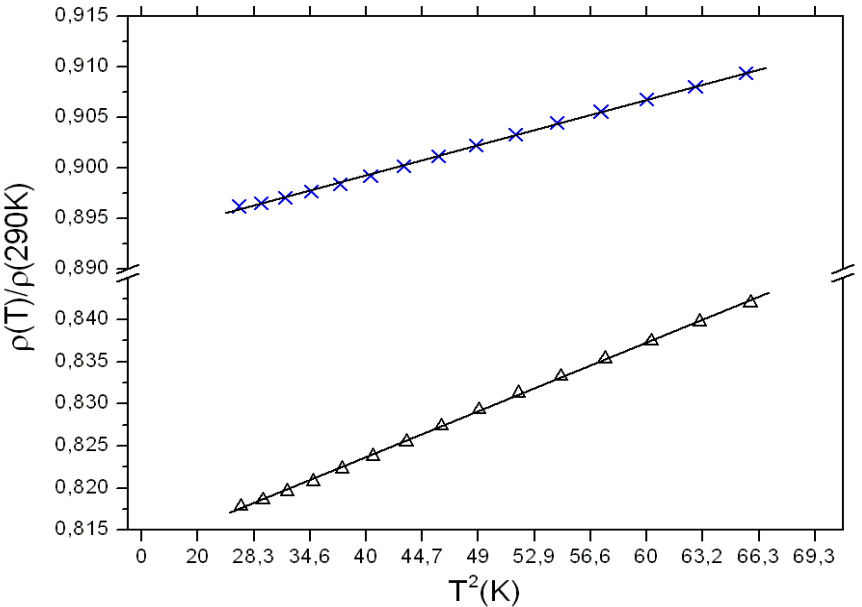
- Dominantan je doprinos slabe lokalizacije, negativan TCR
- Slabo vidljiva saturacija oko 10 K
- Doprirani uzorak (5% H) ima veću absolutnu vrijednost TCR-a – manja stabilnost uzorka

- Ovisnost  $\rho \sim T$  području 25-100 K
- $\tau_i \propto T^{-p}$ ,  $p=2$
- Na  $T > 100$  K ovisnost  $\rho \sim T^{1/2}$   
 $p=1$

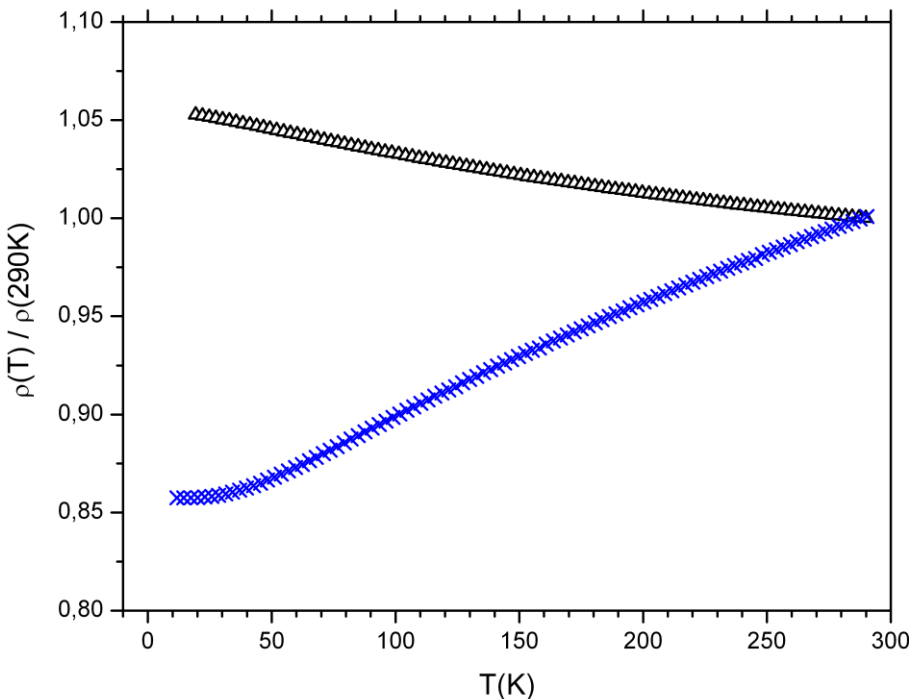


# Otpornost aniliranih uzoraka

- Anilirani uzorci  $Zr_{80}Ni_{20}$  imaju pozitivan TCR
- Uzorak grijan manjom brzinom ima veći TCR, oba su grijana do ispod drugog egzoterma (do  $320^{\circ}\text{C}$ )
- Debyeva temperatura  $\Theta_D$  za ove uzorke je blizu  $T=200 \text{ K}$
- Linearna ovisnost za  $T > \Theta_D$ , iznad  $200 \text{ K}$



- Ovisnost  $\rho \sim T^2$  niskim temperaturama ( $T < \Theta_D$ )
- U skladu sa Ziman-Faberovom teorijom (Nagelov model) gdje je predviđena takva ovisnost



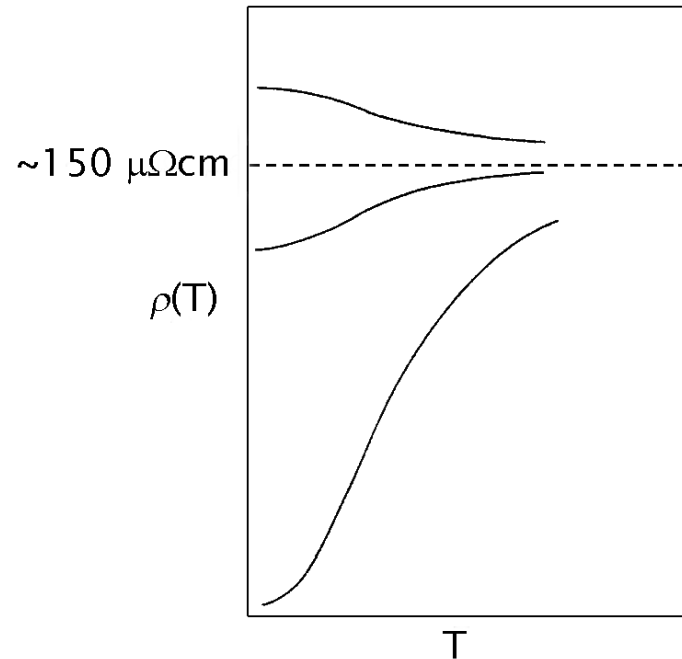
- Usporedba relativne otpornosti staklastog i aniliranog uzorka (dopiranih vodikom,  $x = 0.05$ )
- Staklasti uzorak:  
 $\rho(290K) = (170 \pm 10) \mu\Omega\text{cm}$
- Anilirani uzorak ( $s=10 \text{ K/min}$ ):  
 $\rho(290K) = (100 \pm 10) \mu\Omega\text{cm}$

- Ponašanje je u skladu s Mooijevom korelacijom koja predviđa negativan TCR za otpornosti veće od  $150 \mu\Omega\text{cm}$  i pozitivan TCR za manje vrijednosti
- Poslijedica kristalizacije – smanjenje otpornosti i promjena predznaka TCR-a

# Moojeva korelacija

- Slijedi iz eksperimentalnih opažanja vodljivosti metalnih stakala

1. Otpornost stakala  $\rho > 100 \mu\Omega\text{cm}$  je neosjetljiva na detalje elektronske strukture i atomskog rasporeda
2. Negativan temperturni koeficijent otpornosti (TCR) stakala otpornosti  $\rho > 150 \mu\Omega\text{cm}$
3. Saturacija otpornosti pri  $\rho = 150$ - $200 \mu\Omega\text{cm}$  na visokim temperaturama



- Takvo ponašanje je posljedica približavanja srednjeg slobodnog puta međuatomskim razmacima

# Ziman-Faberova teorija

- Temelji se na Drudeovom modelu
- Primjenjiva na stakla niske otpornosti i kristalinične metale
- Elektroni su opisani ravnim valovima, vektora  $\vec{k}$ , s ravnim slobodni put je veći od međuatomskih udaljenosti
- Vrijeme relaksacije – recipročno vjerojatnosti prijelaza

- Strukturni faktor 
$$\frac{1}{\tau} = \int (1 - \cos \theta) W(\theta) d\Omega$$
- Kvadrat matričnog faktora 
$$S(\vec{q}) = \frac{1}{N} \langle |\sum_i e^{i\vec{q}\vec{R}_i}|^2 \rangle$$
 je 
$$\vec{R}_i = \vec{l}_i + \vec{u}_i$$
- Otpornost
- Ziman i Faberov 
$$\rho = \frac{12\pi V_0}{e^2 \hbar \nu_F^2} \int_0^1 S(\vec{q}) |\nu(\vec{q})|^2 \left(\frac{q}{2k_F}\right)^3 d\left(\frac{q}{2k_F}\right)$$
 vode parcijalne strukturne faktore i koncentracije komponenti

- Za oblik struktornog faktora bitan je položaj fermijevog valnog vektora tekućih metala ili stakala,  $2k_F$

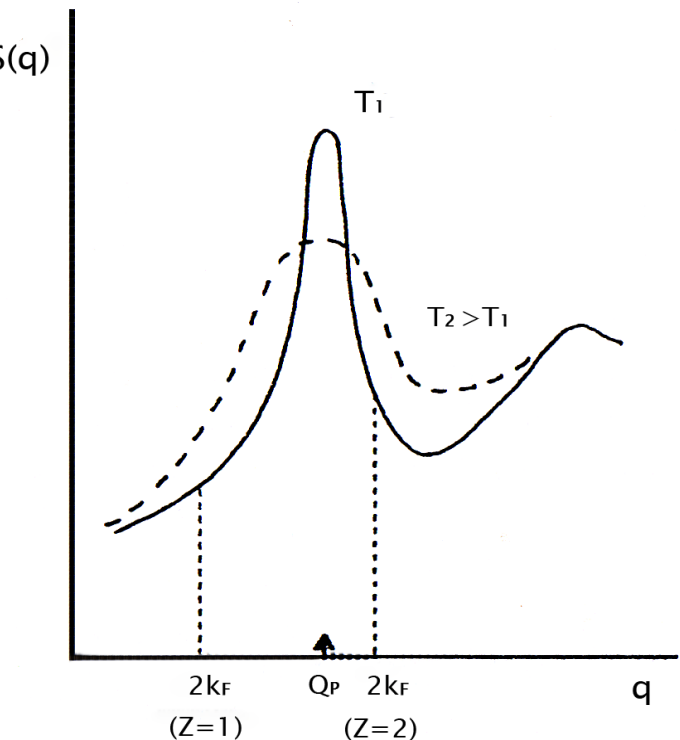
$$k_F = \left( \frac{3\pi^2 Z}{V_0} \right)^{\frac{1}{3}}$$

- Za prikladnu opis stakala uvodi se rezonantno raspršenje vodljivih elektrona na 3d-vrpci  
 $v(q) \rightarrow t(k, k')$
- Cote i Meisel uvode strukturni faktor otpornosti, a Nagel koristi oblik

$$S^p(q) \simeq 1 + [S_{T=0}(q) - 1] e^{-2[W(T) - W(0)]}$$

$$W(T) \simeq W(0) \left[ 1 + \frac{2}{3}\pi^2 \left( \frac{T}{\Theta_D} \right)^2 \right], \quad T \ll \Theta_D$$

$$\simeq W(0) \left[ 1 + \frac{2}{3}\pi^2 \left( \frac{T}{\Theta_D} \right) \right], \quad T \gg \Theta_D$$



Strukturni faktor tekućih metala i metalnih stakala

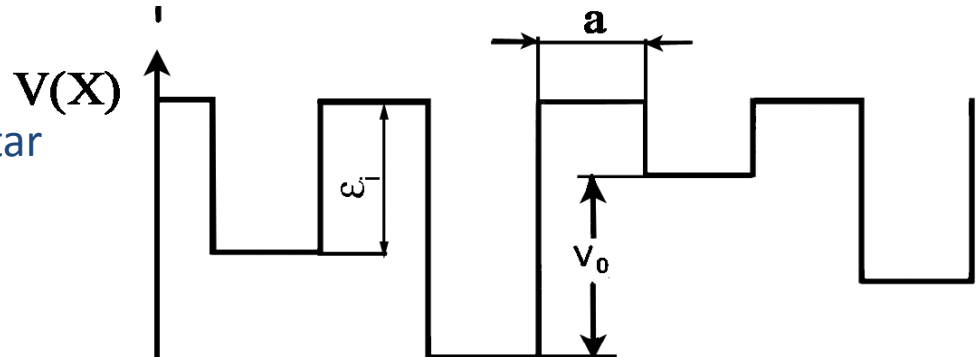
$$\rho \sim T^2$$

$$\rho \sim T$$

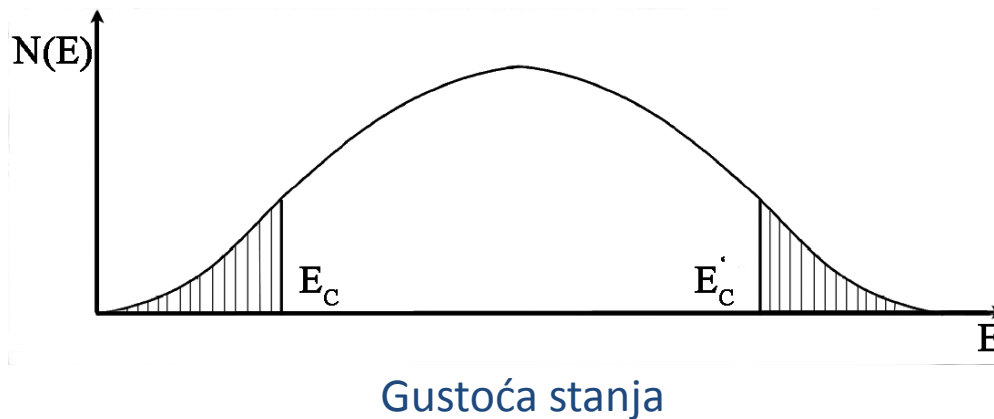
# Kvantni doprinosi

- Andersonov model lokalizacije – temeljen na nasumičnosti potencijala amorfne tvari

- Mjera nereda je interval  $W$  unutar kojeg su raspoređene energije  $\varepsilon_i$

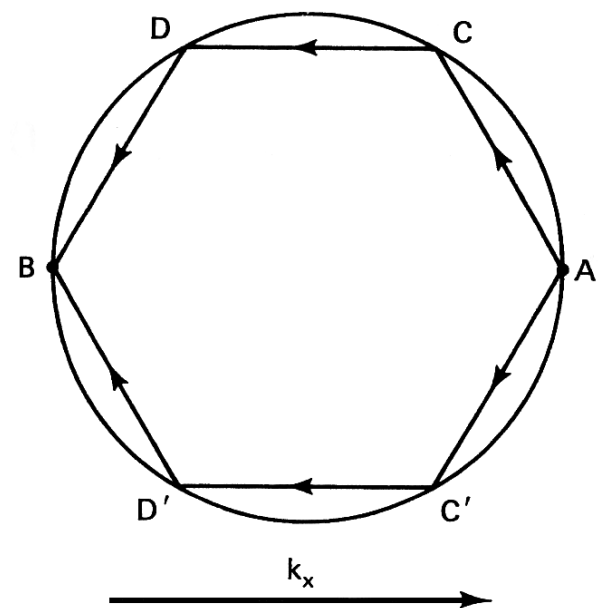


- Hamiltonian sustava 
$$H = \sum_i \epsilon_i |i\rangle\langle i| + \sum_{i,j \neq 0} I(j) |i\rangle\langle i+j|$$
- Pojava lokalizacije Blochovih stanja i povećanja otpornosti



- **Slaba lokalizacija** – posljedica interferencije raspršenih parcijalnih valnih funkcija
- Amplituda raspršenog elektrona je dvostruko veća nego u klasičnom slučaju  $|C + C'|^2 = |C|^2 + |C'|^2 + |CC'^* + C^*C'| = 4|C|^2$
- Koherenciju narušava neelastično raspršenje ( $\tau_i$ ), stoga je ona moguća za  $\tau < \tau_i$
- Temperaturna ovisnost  $\tau_i \propto T^{-p}$ .  
 $2 < p < 4$  za  $T < \Theta_D$
- Doprinos spin-orbit interakcije:  $\tau_{SO}$
- Vodljivost:  

$$\sigma_{WL}(T) = \frac{e^2}{2\pi\hbar} \left[ 3 \left( \frac{1}{D\tau_{SO}} + \frac{1}{4D\tau_i} \right)^{1/2} - \left( \frac{1}{4D\tau_i} \right)^{1/2} \right]$$
- Elektron-elektron interakcija – doprinosi na niskim temperaturama, blizu  $T_c$ , doprinos u Cooperovom i difuznom kanalu



# Model električne vodljivosti u polianilinu

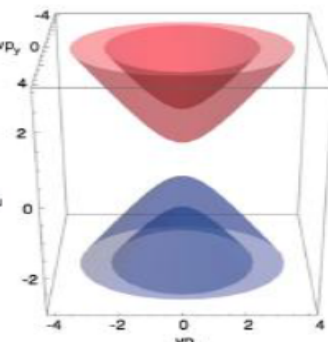
- Doprani polianilin posjeduje veliki stupanj strukturalnog nereda, stanja na Fermijevoj energiji su likalizirana
- Vodljivost je jedino moguća fononski potpomognutim preskocima između lokaliziranih stanja
- Vodljivost je opisana Mott-ovim modelom vođenja mehanizmom preskoka varijabilnog dosega (VRH)
- Preskoci su varijabilnog dosega jer vjerojatnost preskoka ovisi o dva parametra: - udaljenost između lokaliziranih stanja
  - razlici energija između lokaliziranih stanja



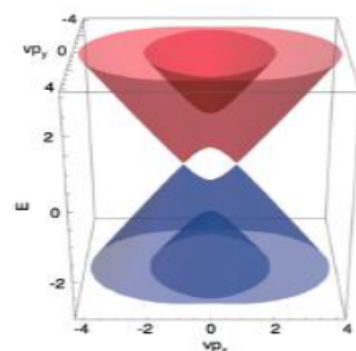
# Magnetski moment sile u topološkim polumetalima

## Topološki polumetali

**Topološki polumetali** → valentna i vodljiva vrpca dodiruju se u **diskretnim točkama ili linijama** u 3D. Oko mesta dodira disperzija je **linearna**.

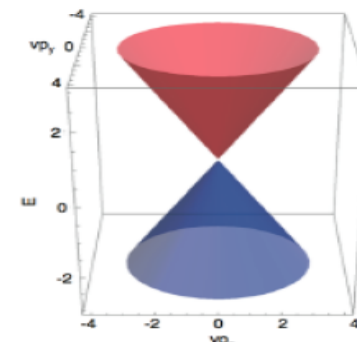


**Poluvodič  
(maseni Dirac)**



**Weylov polumetal**  
➤ Par dvostruko degeneriranih točaka **suprotnih kiralnosti**.

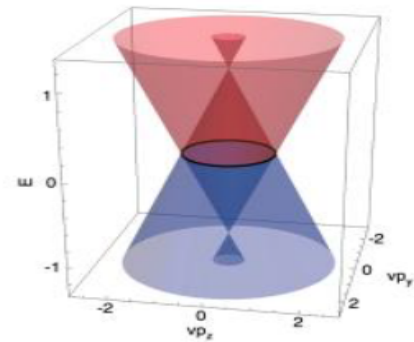
$$H = \pm \hbar v_F \vec{k} \cdot \vec{\sigma}$$



**Diracov polumetal**

- Četverostruko degenerirana točka ( $\times 2$ ).
- Dvije Weylove točke na istom  $\vec{k}$ .

$$H = \hbar v_F \begin{pmatrix} \vec{\sigma} \cdot \vec{k} & 0 \\ 0 & -\vec{\sigma} \cdot \vec{k} \end{pmatrix}$$

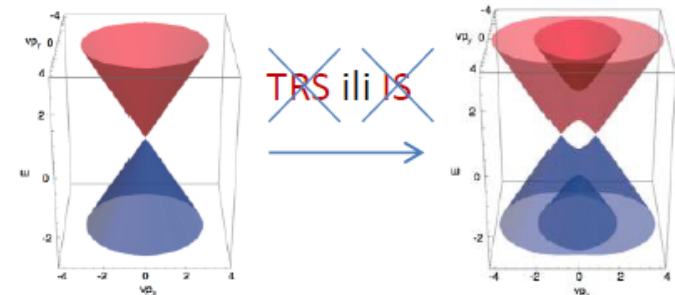
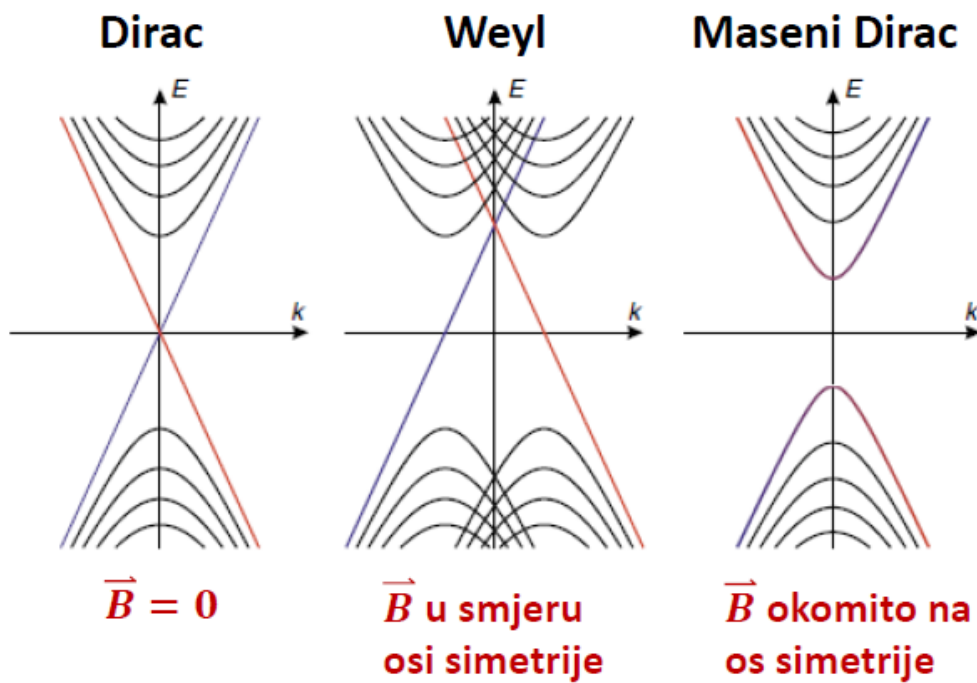


**Linijski Diracov polumetal**

- Vrpce se dodiruju duž linija.

$E_F$  na, ili što bliže točkama dodira → **Weylovi/Diracovi fermioni**

# Diracov polumetal u magnetskom polju



$\vec{B}$  slama simetriju na vremensku inverziju i, ovisno o smjeru, simetriju koja čuva Diracovu točku.

Landauovi nivoi:

$$\varepsilon_{n,k} = \begin{cases} \frac{\hbar e B}{m} (n + \gamma) + \frac{\hbar^2 k_z^2}{2m} & \text{Trivial } (\gamma = \frac{1}{2}) \\ \hbar v_F \sqrt{2B(n + \gamma) + k_z^2} & \text{Weyl } (\gamma = 0) \\ \hbar v_F \sqrt{2B(n + \gamma + C^2 \sin^2 \theta) + k_z^2} & \text{Dirac } (\gamma = 0) \end{cases}$$

$\theta$  je kut između  $\vec{B}$  i osi simetrije koja čuva Diracove točke

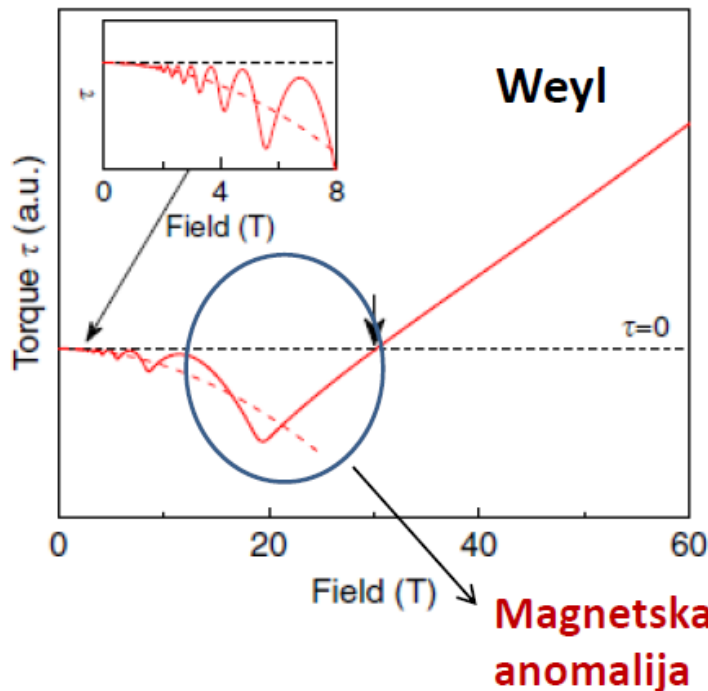
# Diracov polumetal u magnetskom polju

## Landauovi nivoi

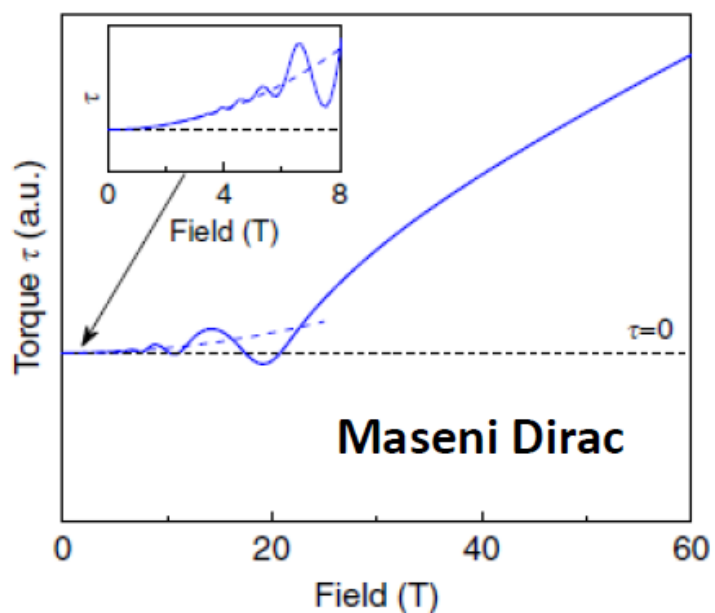
$$\varepsilon_{n,k} = \begin{cases} \frac{\hbar eB}{m}(n + \gamma) + \frac{\hbar^2 k_z^2}{2m} & \text{Trivial } (\gamma = \frac{1}{2}) \\ \hbar v_F \sqrt{2B(n + \gamma) + k_z^2} & \text{Weyl } (\gamma = 0) \\ \hbar v_F \sqrt{2B(n + \gamma + C^2 \sin^2 \theta) + k_z^2} & \text{Dirac } (\gamma = 0) \end{cases}$$

## Magnetizacija u kvantnom limitu ( $n = 0$ )

$$M_{n=0} = -\frac{\partial \varepsilon_{0,k}}{\partial B}$$
$$\vec{\tau} = \vec{M} \times \vec{B}$$



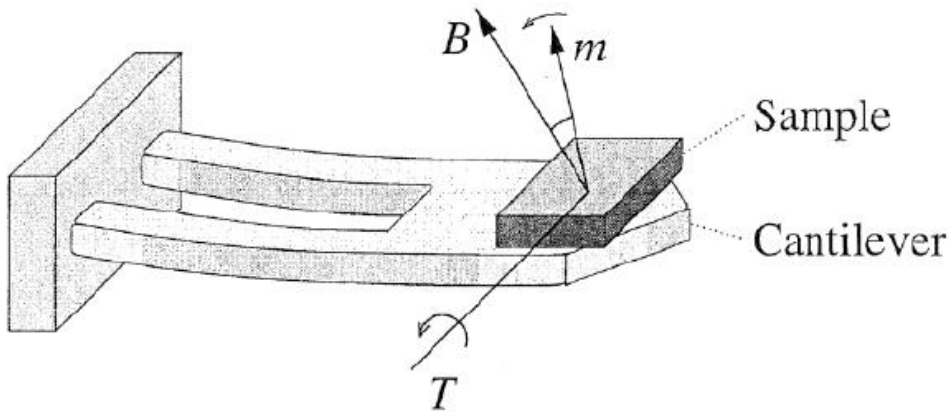
Simulirani  $\vec{\tau}$  za Weylov i maseni Diracov polumetal u kvantnom limitu.



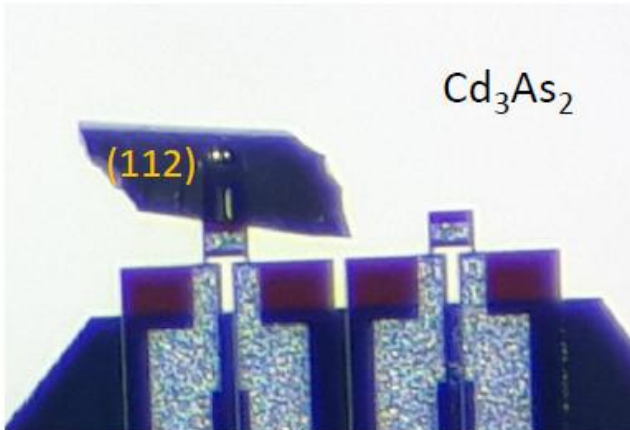
Preuzeto iz Moll, P. J. et al (2016). *Nature Communications*.

# Mjerenje magnetskog momenta sile

## Metoda piezopoluge

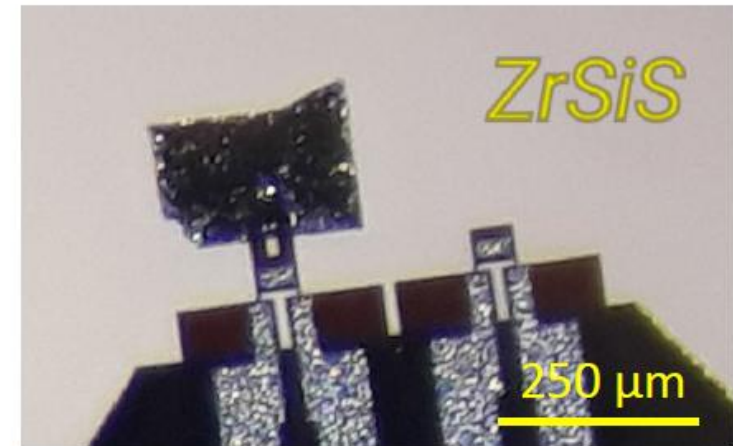


Mjeri se otpor piezootpornog senzora na polugi.



Magnetski anizotropan uzorak.

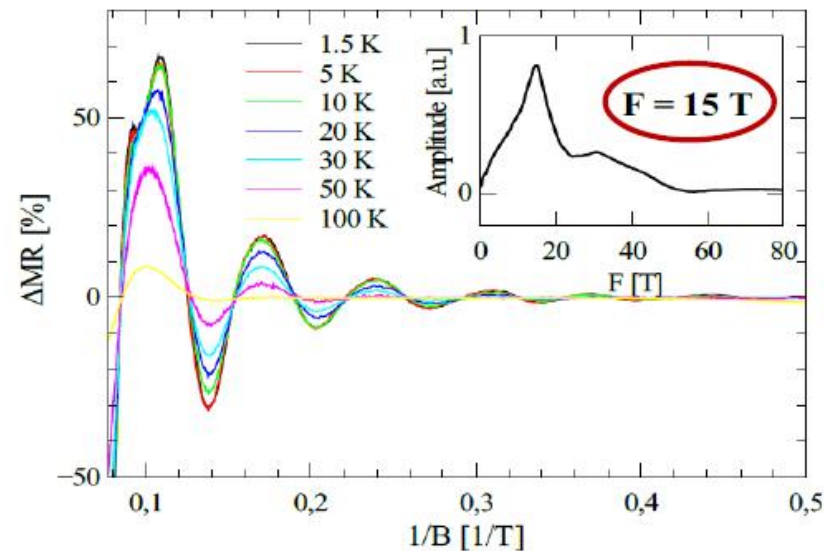
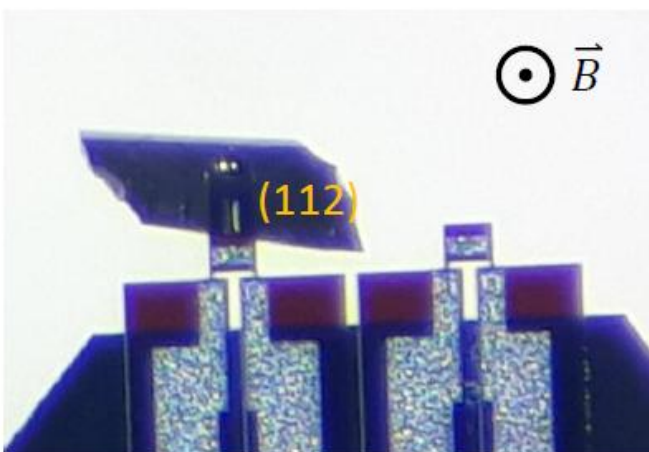
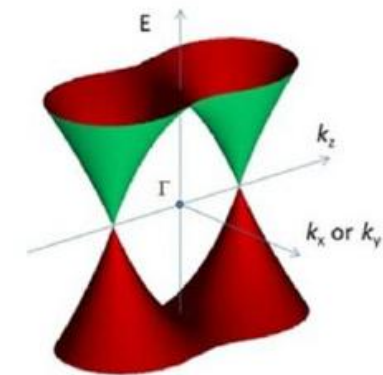
$$\vec{\tau} = \vec{M} \times \vec{B} \propto B^2$$



# $\text{Cd}_3\text{As}_2$

## $\text{Cd}_3\text{As}_2$

- Diracov polumetal.
- Par Diracovih točaka na osi rotacijske simetrije.

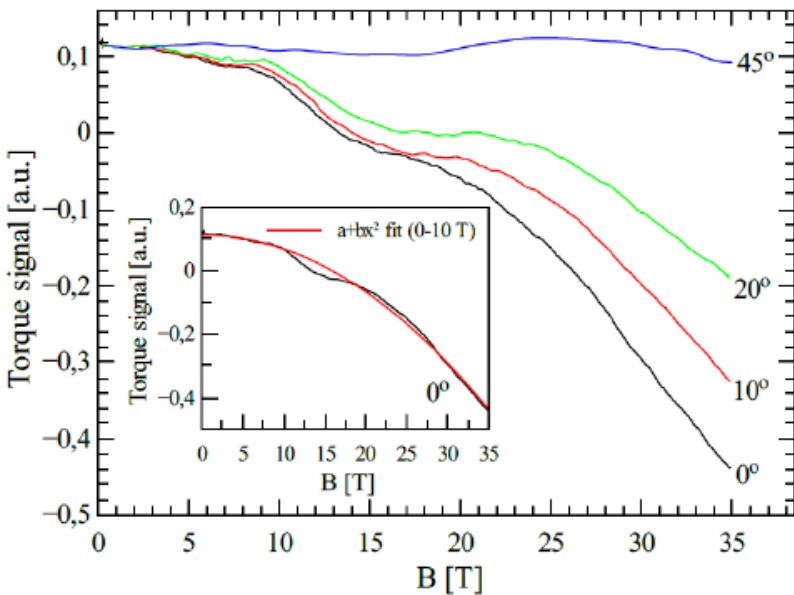


Kvantne oscilacije u magnetootporu  $\text{Cd}_3\text{As}_2$ .

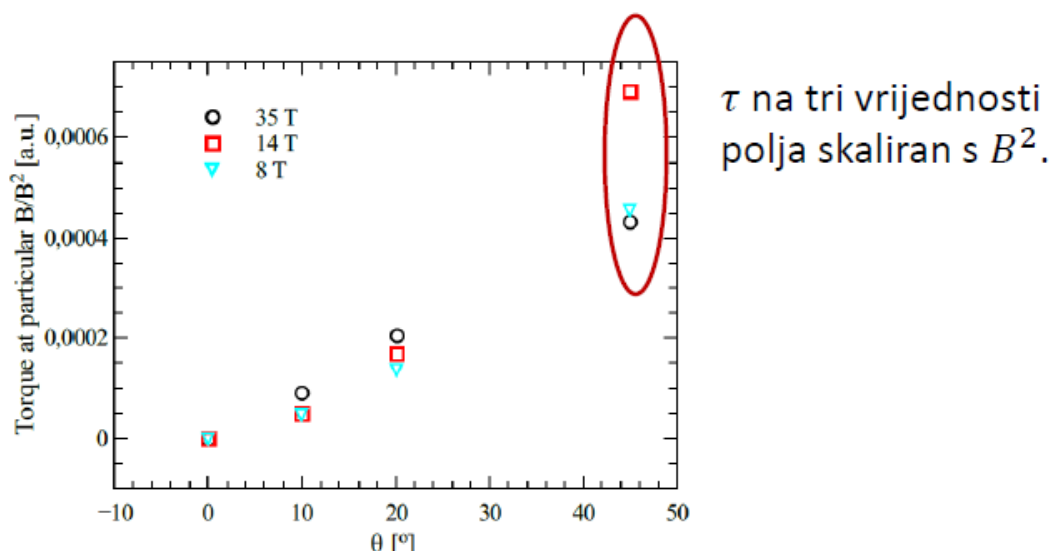
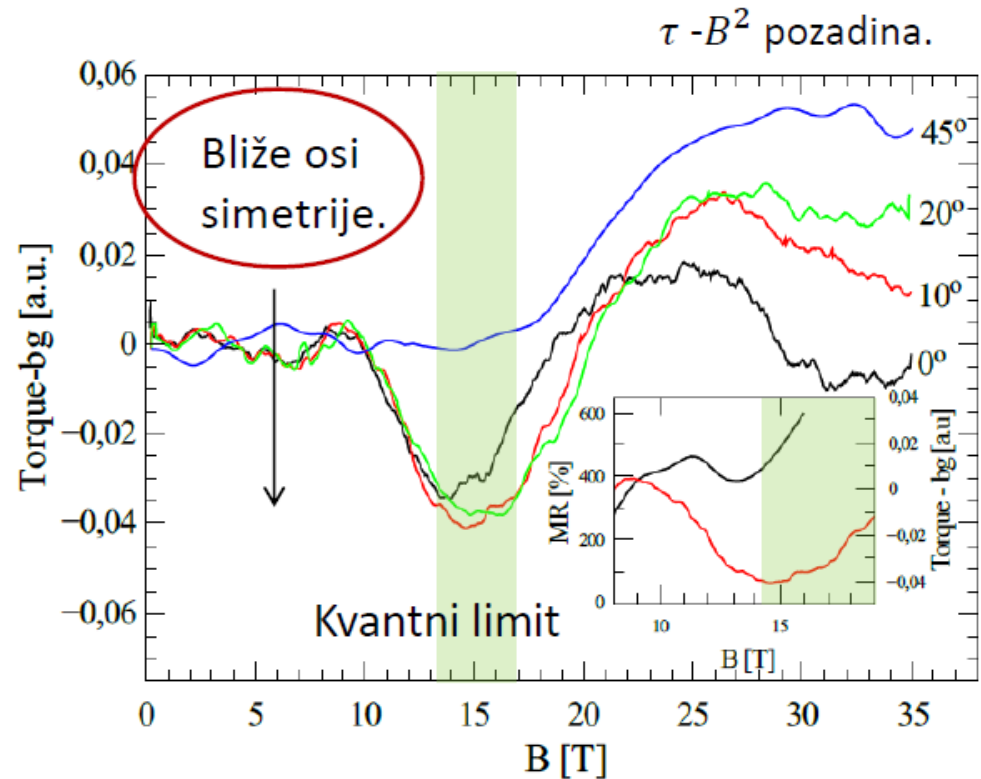
$\bar{\tau}$  je mjerena na 2 K u poljima do 35 T za različite kutove  $\theta$  između polja i normale na (112) ravni.

# $\text{Cd}_3\text{As}_2$

Sirovo mjerjenje  $\tau$  s  $B^2$  ovisnošću.



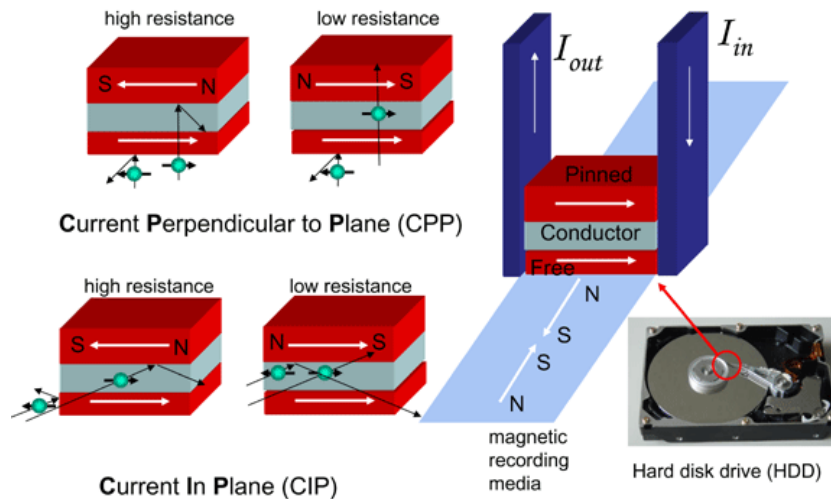
Vidljiva je kutno ovisna magnetska anomalija oko kvantnog limita.



$\tau$  na tri vrijednosti polja skaliran s  $B^2$ .

# Primjer znanstvenog otkrića

- The Nobel Prize in Physics 2007 was awarded jointly to **Albert Fert** and **Peter Grünberg** "for the discovery of Giant Magnetoresistance (GMR)"



# Gigantski magnetootpor

- Članak iz 1988.g. : M. N. Baibich, J. M. Broto, **A. Fert**, F. Nguyen Van Dau, F. Petroff, P. Etienne, G. Creuzet, A. Friederich, and J. Chazelas, **Giant Magnetoresistance of (001)Fe/(001)Cr Magnetic Superlattices**, Phys. Rev. Lett. **61**, 2472 (1988)
- ideja iz 1970. g. – korištenje spinski polariziranih struja
- koncept ostvaren tek 1988. g. razvojem tehnologije (MBE) – tanki slojevi magnetskih i

## Giant Magnetoresistance of (001)Fe/(001)Cr Magnetic Superlattices

M. N. Baibich,<sup>(a)</sup> J. M. Broto, A. Fert, F. Nguyen Van Dau, and F. Petroff  
*Laboratoire de Physique des Solides, Université Paris-Sud, F-91405 Orsay, France*

P. Eitenne, G. Creuzet, A. Friederich, and J. Chazelas  
*Laboratoire Central de Recherches, Thomson CSF, B.P. 10, F-91401 Orsay, France*  
 (Received 24 August 1988)

We have studied the magnetoresistance of (001)Fe/(001)Cr superlattices prepared by molecular-beam epitaxy. A huge magnetoresistance is found in superlattices with thin Cr layers: For example, with  $t_{\text{Cr}} = 9 \text{ \AA}$ , at  $T = 4.2 \text{ K}$ , the resistivity is lowered by almost a factor of 2 in a magnetic field of 2 T. We ascribe this giant magnetoresistance to spin-dependent transmission of the conduction electrons between Fe layers through Cr layers.

PACS numbers: 75.50.Rr, 72.15.Gd, 75.70.Cn

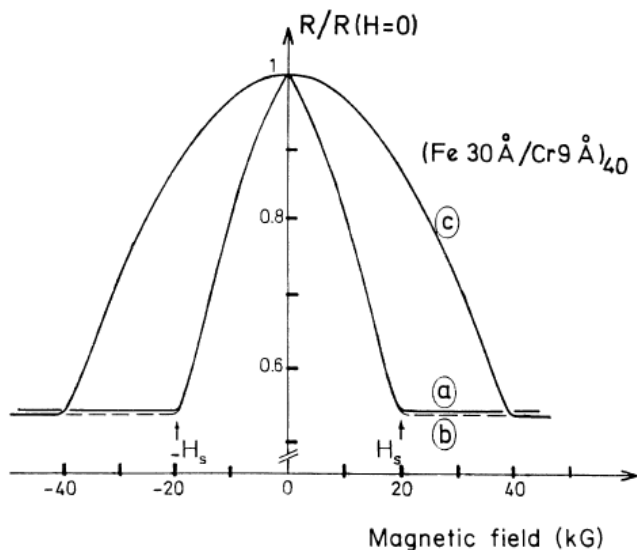
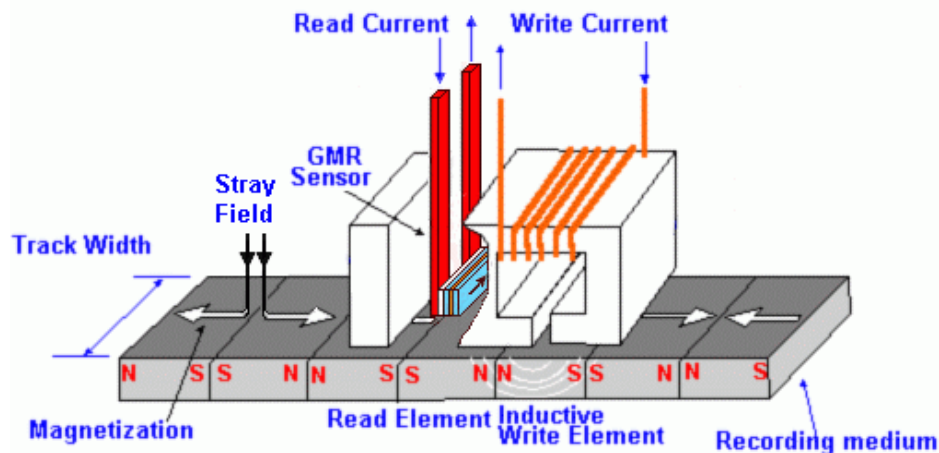
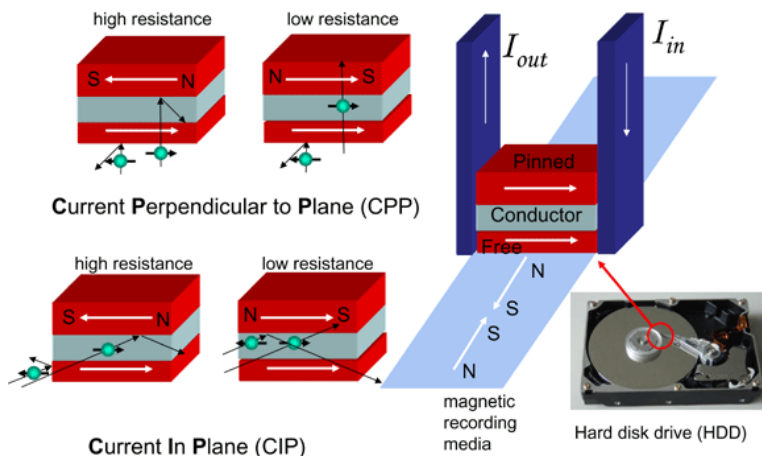


FIG. 2. Magnetoresistance of a  $[(\text{Fe } 30 \text{ \AA})/(\text{Cr } 9 \text{ \AA})]_{40}$  superlattice of 4.2 K. The current is along [110] and the field is in the layer plane along the current direction (curve *a*), in the layer plane perpendicular to the current (curve *b*), or perpendicular to the layer plane (curve *c*). The resistivity at zero field is  $54 \mu\Omega \text{ cm}$ . There is a small difference between the curves in increasing and decreasing field (hysteresis) that we have not represented in the figure. The superlattice is covered by a 100-Å Ag protection layer. This means that the magnetoresistance of the superlattice alone should be slightly higher.

# Gigantski magnetootpor

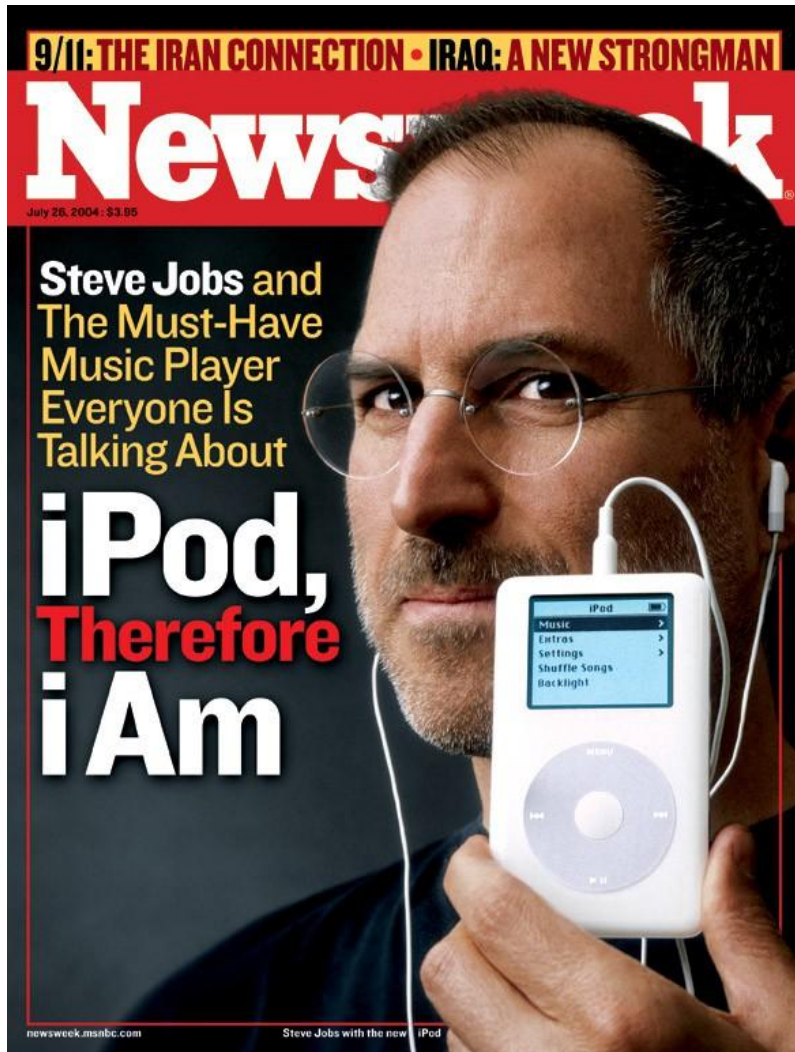
- rođena je **spintronika**
- omogućen razvoj sve manjih tvrdih diskova

Giant Magnetoresistance (GMR)

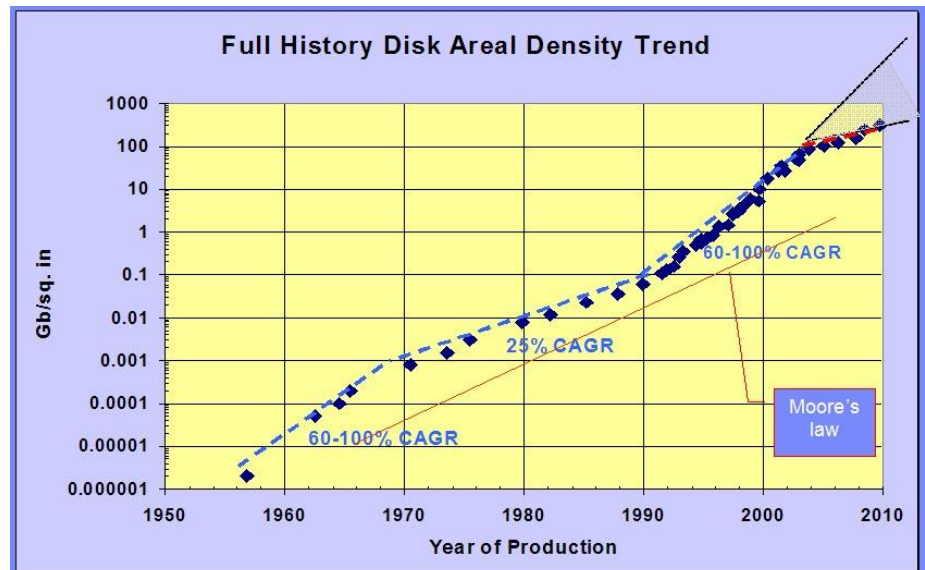


- usavršavanje preuzela **industrija**
- Nakon toga nagradio *the greatest benefit on*

# Gigantski magnetootpor

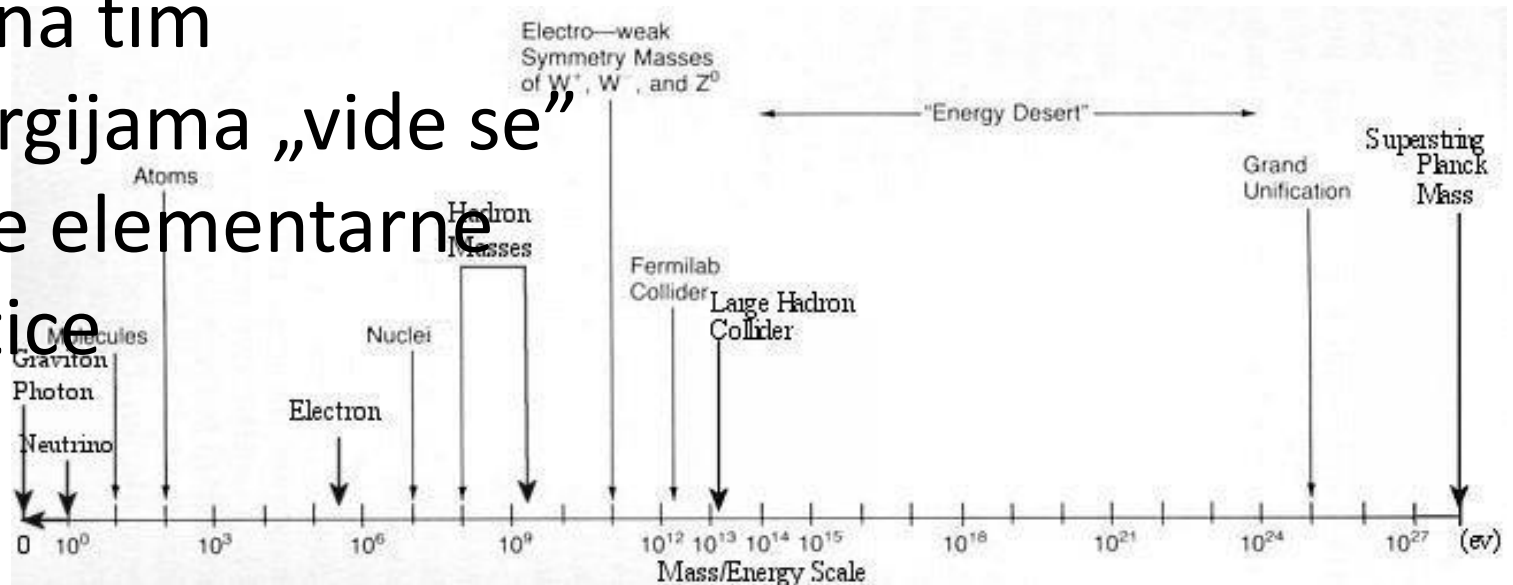
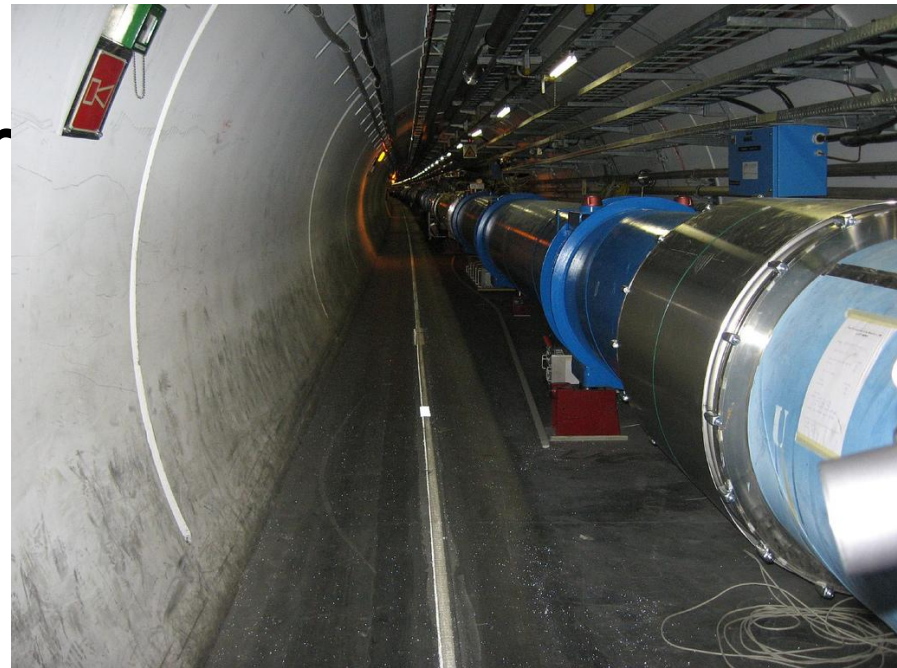


The small white player has a 1,000 song capacity thanks to its 5GB hard drive



# Primjer

- ubrzavanje čestica (protona) do 6.5 TeV (13 TeV kombinirano)
- tek na tim energijama „vide se“ neke elementarne čestice



# Važnost eksperimentalne fizike za šire društvo

- J. Liebing (~1850. g.): ...Stoga, što znamo prirodi, ovisi o onome što možemo učiniti, a to ovisi o uređajima kojima raspolažemo, materijalima kojima raspolažemo za gradnju uređaja i vještini kojom koristimo te uređaje.”
- napredna tehnologija – proizvodnja u „laboratorijskim” uvjetima: fizika, kemija, biologija
- zasnovana na znanstvenim otkrićima i koristi uređaje razvijene za eksperimentalnu fiziku

# Primjer: proizvodnja procesora

